The QCD strong coupling from hadronic τ decays

Universitat Autònoma de Barcelona

Dirk Hornung

Day Month Year

Abstract

Acknowledgements

Notations

Abbreviations are given in small-caps. E.g SM instead of SM (following [7]).

Every abbreviation is indexed at the end of this thesis.

Important formulas are emphasised by a grey background (like in [54]).

Chapter 1

Introduction

In particle physics we are concerned about small objects and their interactions. The smallest of these objects are referred to as *elemental particles*. Their dynamics are governed by the laws of nature. These laws are organised through symmetries, which are currently best described by the *Standard Model* (SM).

The SM classifies all known elementary particles and describes three of the four fundamental forces: the electromagnetic, weak and strong force. The particles representing matter are contained in two groups of fermionic, spin-1/2 particles. The former group, the leptons consist of: the electron (e), the muon (μ), the tau (τ) and their corresponding neutrinos ν_e, ν_μ and ν_τ. The latter group, the quarks contain: u, d (up and down, the so called light quarks), s (strange), c (charm), b (bottom or beauty) and t (top or truth). The three fundamental forces, the SM differentiates, are described through their carrier particles, the so-called bosons: the photon for the electromagnetic, the Z-or *W*-Boson for the weak and the gluon (g) for the strong interaction. and strong (g gluon) interactions. The before mentioned Leptons solely interact through the electromagnetic and the weak force (also referred to as electroweak interaction), whereas the quarks additionally interact through the strong force. A short summary of the taxonomy of the SM can be seen in fig. 1.1

From a more mathematical point of view the SM is a gauge *Quantum Field Theory* (QFT). is the combination of *classical field theory*, *special relativity* and *quantum mechanics*. Its fundamental objects are ruled through its gauge-group $SU(3) \times SU(2) \times U(1)$. Each of its subgroups introduces a global and a local gauge symmetry. The global symmetry introduces the charges, which the

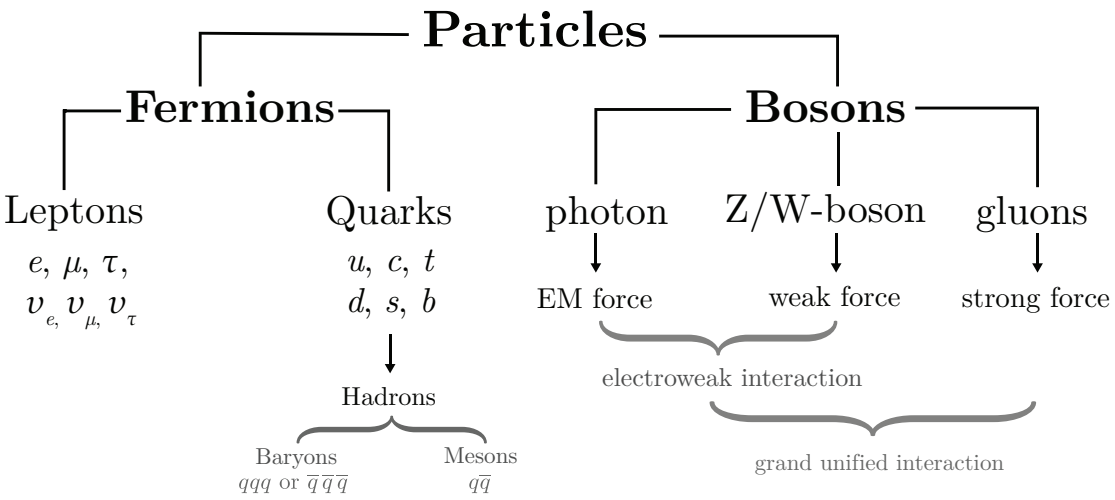

Figure 1.1: Taxonomy of the Standard Model.

fields are carrying. The local symmetry introduce the gauge-fields, which represent the previously mentioned force carriers. Naively every subgroup[1] of the gauge-group of the standard model is responsible for one of the three forces:

U(1) the *abelian* gauge group governs the representation of *quantum electrodynamics* (QED), which is commonly known as the electric force. Its global and local symmetry introduces the electric charge and the photon-field.

SU(2) Is the *non-abelian* symmetry group responsible for the weak-interaction. It introduces the W^+, W^- and Z bosons and the weak charge. The gauge groups U(1) and SU(2) have been combined to the *electroweak interaction*.

SU(3) The SU(3)-group is also *non-abelian* and governs the strong interactions, which are summarised in the theory of *Quantum Chromodynamics* (QCD). The group yields the three colour charges and due to its eight-dimensional adjoint-representation, eight different gluons.

Unfortunately we are still not able to include gravity, the last of the four forces, into the SM. There have been attempts to describe gravity through QFT with

[1] Actually U(1) and SU(2) have to be regarded as combined group to be mapped to the electromagnetic-and weak-force in form of the electroweak interaction.

the graviton, a spin-2 boson, as mediator, but there are unsolved problems with the renormalisation of general relativity (GR). Until now GR and quantum mechanics (QM) remain incompatible.

Apart from gravity no being included, the SM has a variety of flaws. One of them is being dependent on many parameters, which have to be measured accurately to perform high-precision physics. In total the Lagrangian of the SM contains 19 parameters. These parameters are represented by ten masses, four CKM-matrix parameters, the QCD-vacuum angle, the Higgs-vacuum expectation value and three gauge coupling constants. Highly accurate values with low errors are crucial for theoretical calculated predictions. One of the major error inputs of every theoretical output are uncertainties in these parameters. In this work we will focus on one of the parameters, namely the strong coupling α_s.

The strong coupling is currently measured in six different ways: through τ-decays, QCD-lattice computations, deep inelastic collider results and electroweak precision fits [59]. We have plotted the values of each of the methods in fig. 1.2. During this work we will focus on the subfield of τ-decays to measure the value of the strong coupling $\alpha_s(m_\tau)$ at the τ-scale. We will see that in QCD the value of the coupling "constant" depends upon the scale. The τ is an elementary particle with negative electric charge and a spin of $1/2$. Together with the lighter electron and muon it forms the group of charged Leptons[2]. Even though it is an elementary particle it decays via the weak interaction with a lifetime of $\tau_\tau = 2.9 \times 10^{-13}$ s and has a mass of $1776.86(12)\,MeV$[59]. It is furthermore the only lepton massive enough to decay into hadrons, thus of interest for our QCD study. The final states of a decay are limited by conservation laws. In case of a τ-decay they must conserve the electric charge (-1) and invariant mass of the system. Thus, we can see from the corre-

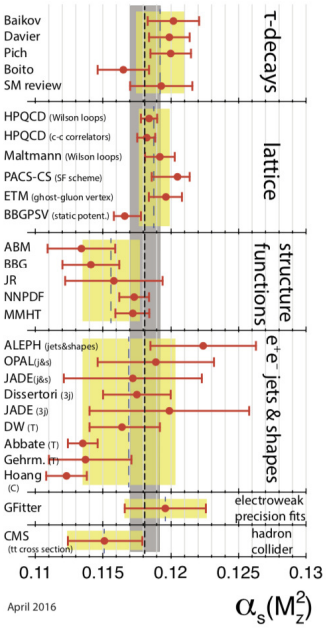

Figure 1.2: The six different subfields and their results for measuring the strong coupling α_s [59].

[2]Leptons do not interact via the strong force.

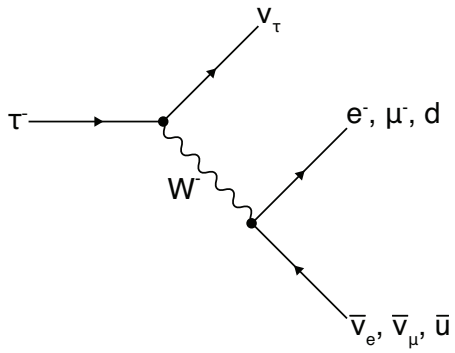

Figure 1.3: Feynman diagram of common decay of a τ-lepton into pairs of lepton-antineutrino or quark-antiquark by the emission of a *W boson*.

Name	Symbol	Quark content	Rest mass (MeV)
Pion	π^-	$\bar{u}d$	139.570 61(24) MeV
Pion	π^0	$(u\bar{u} - d\bar{d})/\sqrt{2}$	134.9770(5) MeV
Kaon	K^-	$\bar{u}s$	493.677(16) MeV
Kaon	K^0	$d\bar{s}$	497.611(13) MeV
Eta	η	$(u\bar{u} + d\bar{d} - 2s\bar{s})/\sqrt{6}$	547.862(17) MeV

Table 1.1: List of mesons produced by a τ-decay. Rare final states with branching Ratios smaller than 0.1 have been omitted. The list is taken from [22] with corresponding rest masses taken from [59].

sponding Feynman diagram fig. 1.3 [3], that the τ decays by the emission of a *W*-boson and a tau-neutrino ν_τ into pairs of $(e^-, \bar{\nu}_e), (\mu^-, \bar{\nu}_\mu)$ or $(q, \bar{q})$. We are foremost interested into the hadronic decay channels, meaning τ-decays that have quarks in their final states. Quarks have never been measured isolated, but appear always in combination of *mesons* and *baryons*. Due to its mass of $m_\tau \approx 1.8\,GeV$ the τ-particle decays into light mesons (pions-π, kaons-K, and eta-η, see table 1.1), which can be experimentally detected. The hadronic τ-decay provides one of the most precise ways to determine the strong coupling [48] and is theoretically accessible to high precision within the framework of QCD.

[3]The τ-particle can also decay into strange quarks or charm quarks, but these decays are rather uncommon due to the heavy masses of s and c.

The theory describing strong interactions is QCD. As the name suggest[4] QCD is characterised by the colour charge and is a non-abelian gauge theory with symmetry group $SU(3)$. Consequently every quark has next to its type one of the three colours blue, red or green and the colour force is mediated through eight gluons, which each being bi-coloured[5], interact with quarks and each other. The strength of the strong force is given by the coupling constant α_s, which depends on the renormalisation-scale μ. We often chosen the renormalisation-scale in a way that the coupling constant $\alpha_s(q)$ depends on the energy q^2. Thus the coupling varies with energy. It increases for low and decreases for high energies[6]. This behaviour has two main implications. The first one states, that for low energies the coupling is too strong for isolated quarks to exist. Until now we have not been able to observe an isolated quark and all experiments can only measure quark compositions. These bound states are called *hadrons* and consist of two or three quarks [7], which are referred to as mesons[8] or baryons [9] respectively. This phenomenon, of quarks sticking together as hadrons is referred to as *confinement*. As the fundamental degrees of freedom of QCD are given by quarks and gluons, but the observed particles are hadrons we need to introduce the assumption of *quark-hadron duality* to match the theory to the experiment. This means that a physical quantity should be similarly describable in the hadronic picture or quark-gluon picture and that both descriptions are equivalent. As we will see in our work quark-hadron duality is violated for low energies. These so-called *duality violations* (DV) have an impact on our strong coupling determinations and can be dealt with either suppression or the inclusion of a model [15]. Throughout this work we will favour and argument for the former approach. The second implication concerns *Perturbative Theory* (PT). The lower the energies we deal with, the higher the value of the strong coupling and the contributions of *Non-Perturbative Theory* (NPT) effects. Currently there are three solutions to deal with *Non-Perturbative* (NP) effects:

- ***Chiral Perturbation Theory*** (CHPT): Introduced by Weinberg [63] in the

[4] Chromo is the Greek word for colour.
[5] Each gluon carries a colour and an anti-colour.
[6] In contrast to the electromagnetic force, where $\alpha(q^2)$ decreases!
[7] There exist also so-called *Exotic hadrons*, which have more than three valence quarks.
[8] Composite of a quark and an anti-quark.
[9] Composite of three quarks or three anti-quarks.

late seventies. CHPT is an effective field theory constructed with a Lagrangian symmetric under a chiral-transformation in the limit of massless quarks. It's limitations are based in the chiral symmetry, which is only a good approximation for the light quarks u, d and in some cases s.

- ***Lattice QCD*** (LQCD): Is the numerical approach to the strong force. Based on the Wilson Loops [65] we treat QCD on a finite lattice instead of working with continuous fields. LQCD has already many applications but is limited due to its computational expensive calculations.

- ***QCD Sum Rules*** (QCDSR): Was also introduced in the late seventies by Shifman, Vainstein and Zakharov [56, 55]. It relates the observed hadronic picture to quark-gluon parameters through a dispersion relation and the use of the *Operator Product Expansion* (OPE), which treats NP effect through the definition of vacuum expectation values, the so-called *QCD condensates*. It is a precise method for extracting the strong coupling α_s at low energies, although limited to the unknown higher order contributions of the OPE.

In this work we focus on the determination of the strong coupling α_s within the framework of QCDSR for τ-decays which has been exploited in the beginning of the nineties by Braaten, Narison and Pich [12]. Within this setup we can measure $\alpha_s(m_\tau^2)$ at the m_τ scale. As the strong coupling gets smaller at higher energies, so do the errors. Thus if we obtain the strong coupling at a low scale we will obtain high precision values at the scale of the Z-boson mass m_Z, which is the standard scale to compare α_s values.

The QCDSR for the determination of α_s, from low energies, contain three major issues.

1. There are two different approaches to treat perturbative and non-perturbative contributions. In particular, there is a significant difference between results obtained using fixed-order (FOPT) or contour improved perturbation theory (CIPT), such that analyses based on CIPT generally arrive at about 7% larger values of $\alpha_s(m_{\tau^2})$ than those based on FOPT [59]. There have been a variety of analyses on the topic been performed [46, 14, 33] and we will favour the FOPT approach, but generously list our results for the CIPT framework.

2. There are several prescriptions to deal with the NP-contributions of higher order OPE condensates. Typically terms of higher dimension have been neglected, even if they knowingly contribute. In this work we will include every necessary OPE term.

3. Finally there are known DV leading to an ongoing discussion of the importance of contributions from DV. Currently there are two main approaches: Either we neglect them, arguing that they are sufficiently suppressed due to *pinched weights* [48] or model DV with sinusoidal exponentially suppressed function [15, 8, 10] introducing extra fitting parameters. We will argue for the former method, implementing pinched weights that sufficiently suppress DV contributions such as having only a negligible effect on our analysis.

In the first chapter of this work we want to summarise the necessary theoretical background for working with the QCDSR. Starting with the basics of QCD we want to motivate the *Renormalisation Group Equation* (RGE), which is responsible for the running of the strong coupling. We then continue with the some aspects of the two-point function and its usage in the dispersion relation, which connects the hadronic picture with the quark-gluon picture. ···

Chapter 2

QCD Sum Rules

The theory of QCD was formulated to find one single framework that describes the many hadrons that exist. Unfortunately making use of *perturbative* QCD (PQCD) is limited. QCD predicts a large coupling constant for low energies. As a consequence we can only ever observe hadrons, but our theoretical foundation is ruled by the DOF of quarks and gluons. To extract QCD parameters (the six quark masses and the strong coupling) from hadrons we need to bridge the quark-gluon picture with the hadron picture. To do so we will introduce the framework of QCDSR.

We will start by setting up the foundations of strong interaction with introducing the QCD-Lagrangian. The QCD-Lagrangian is ruled by the abelian gauge group $SU(3)$. The group implies a energy dependence of the coupling and thus limits the applicability of PT for low energies, where the coupling is large. Next we will focus on the two-point function, which plays a major role in the framework of QCDSR. The two-point function is defined as vacuum-expectation values of two local fields

$$\Pi(s) = \langle \Omega | q(x) q(y) | \Omega \rangle. \tag{2.0.1}$$

We can use it to theoretically describe processes, like τ-decays into hadrons, by matching the quantum numbers of the fields, we choose in specifying the two-point function, to the outgoing hadrons. We will see, that the two-point function $\Pi(q^2)$ is related to hadronic states, by poles for $q^2 > 0$. Here NP-effects become important and we need to introduce the OPE, which handles NP parts through QCD-condensates. The condensates form part of the full physical vacuum and would not exist regarding the perturbative vacuum solely. Con-

sequently the condensates are not accessible trough PT methods and have to be fitted from experiment or calculated with the help of NP tools, like LQCD. Finally we will combine a dispersion relation and Cauchy's theorem to finalise the discussion on the QCDSR with developing the *finite energy sum rules* (FESR), which we will apply to extract the strong coupling from tau-decays into hadrons.

2.1 Quantum-chromodynamics

Since the formulation of QED in the end of the 40's it had been attempted to describe the strong nuclear force as a QFT, which has been achieved in the 70's as QCD [29, 28, 31, 49, 62]. QCD is a renormalisable QFT constructed to describe the strong interaction. Its fundamental fields are given by dirac spinors of spin-1/2, the so-called quarks, with a fractional electric charge of $\pm 1/3$ or $\pm 2/3$. The theory furthermore contains gauge fields of spin 1. These gauge fields are called gluons, do not carry electric charge and are massless. They are the force mediators, which interact with quarks and themselves, because they carry colour charge, in contrast to photons of QED, which interact only with fermions.

The corresponding gauge-group of QCD is the non-abelian group $SU(3)$. Each of the quark flavours u, d, c, s, t and b belongs to the fundamental representation of $SU(3)$ and contains a triplet of fields Ψ.

$$\Psi = \begin{pmatrix} \Psi_1 \\ \Psi_2 \\ \Psi_3 \end{pmatrix} \tag{2.1.1}$$

The labels of the triplet are the colours red, green and blue, which play the role of *colour charge*, similar to the electric charge of QED. The gluons belong to the adjoint representation of $SU(3)$, contain an octet of fields and can be expressed using the Gell-Mann matrices λ_a

$$B_\mu = B_\mu^a \lambda_a \qquad a = 1, 2, \ldots 8 \tag{2.1.2}$$

The classical *Lagrange density* of QCD is given by [67, 43]:

Flavour	Mass
u	2.50(17) MeV
d	4.88(20) MeV
s	93.44(68) MeV
c	1.280(13) GeV
b	4.198(12) GeV
t	173.0(40) GeV

Table 2.1: List of quarks and their masses. The masses of the up, down and strange quark are quoted in the four-flavour theory ($N_f = 2+1+1$ at the scale $\mu = 2\,GeV$ in the $\overline{MS}$. The charm and bottom quark are also taken in the four-flavour theory and in the $\overline{MS}$ scheme, but at the scales $\mu = m_c$ and $\mu =_b$ correspondingly. All quarks except for the top quark are taken from the *Flavour Lattice Averaging Group* [3]. The mass of the top quark is not discussed in [3] and has been taken from [59] from direct observations of top events.

$$\mathcal{L}_{QCD}(x) = -\frac{1}{4}G^a_{\mu\nu}(x)G^{\mu\nu a}(x) + \sum_A \left[\frac{i}{2}\bar{q}^A(x)\gamma^\mu \overleftrightarrow{D}_\mu q^A(x) - m_A \bar{q}^A(x) a^A(x)\right], \tag{2.1.3}$$

with $q^A(x)$ representing the quark fields and $G^a_{\mu\nu}$ being the *gluon field strength tensor* given by:

$$G^a_{\mu\nu}(x) \equiv \partial_\mu B^a_\nu(x) - \partial^a_\nu(x) + g f^{abc} B^b_\mu(x) B^c_\nu(x), \tag{2.1.4}$$

with f^{abc} as *structure constants* of the gauge-group $SU(3)$ and $\overleftrightarrow{D}_\mu$ as covariant derivative acting to the left and to the right. Furthermore we have used $A, B, \ldots = 0, \ldots 5$ as flavour indices, $a, b, \ldots = 0, \ldots, 8$ as colour indices and $\mu, \nu, \ldots = 0, \ldots 3$ as lorentz indices. Explicitly the Lagrangian writes:

$$\begin{aligned}
\mathcal{L}_0(x) = &-\frac{1}{4}\left[\partial_\mu G^a_\nu(x) - \partial_\nu G^a_\mu(x)\right]\left[\partial^\mu G^\nu_a(x) - \partial^\nu G^\mu_a(x)\right] \\
&+ \frac{i}{2}\bar{q}^A_\alpha(x)\gamma^\mu \partial_\mu q^A_\alpha(x) - \frac{i}{2}\left[\partial_\mu \bar{q}^A_\alpha(x)\right]\gamma^\mu q^A_\alpha(x) - m_A \bar{q}^A_\alpha(x) q^A_\alpha(x) \\
&+ \frac{g_s}{2}\bar{q}^A_\alpha(x)\lambda^a_{\alpha\beta}\gamma_\mu q^A_\beta(x) G^\mu_a(x) \\
&- \frac{g_s}{2} f_{abc}\left[\partial_\mu G^a_\nu(x) - \partial_\nu G^a_\mu(x)\right] G^\mu_b(x) G^\nu_c(x) \\
&- \frac{g_s^2}{4} f_{abc} f_{ade} G^b_\mu(x) G^c_\nu(x) G^\mu_d(x) G^\nu_e(x)
\end{aligned} \tag{2.1.5}$$

The first term is the kinetic term for the massless gluons. The next three terms are the kinetic terms for the quark field with different masses for each flavour.

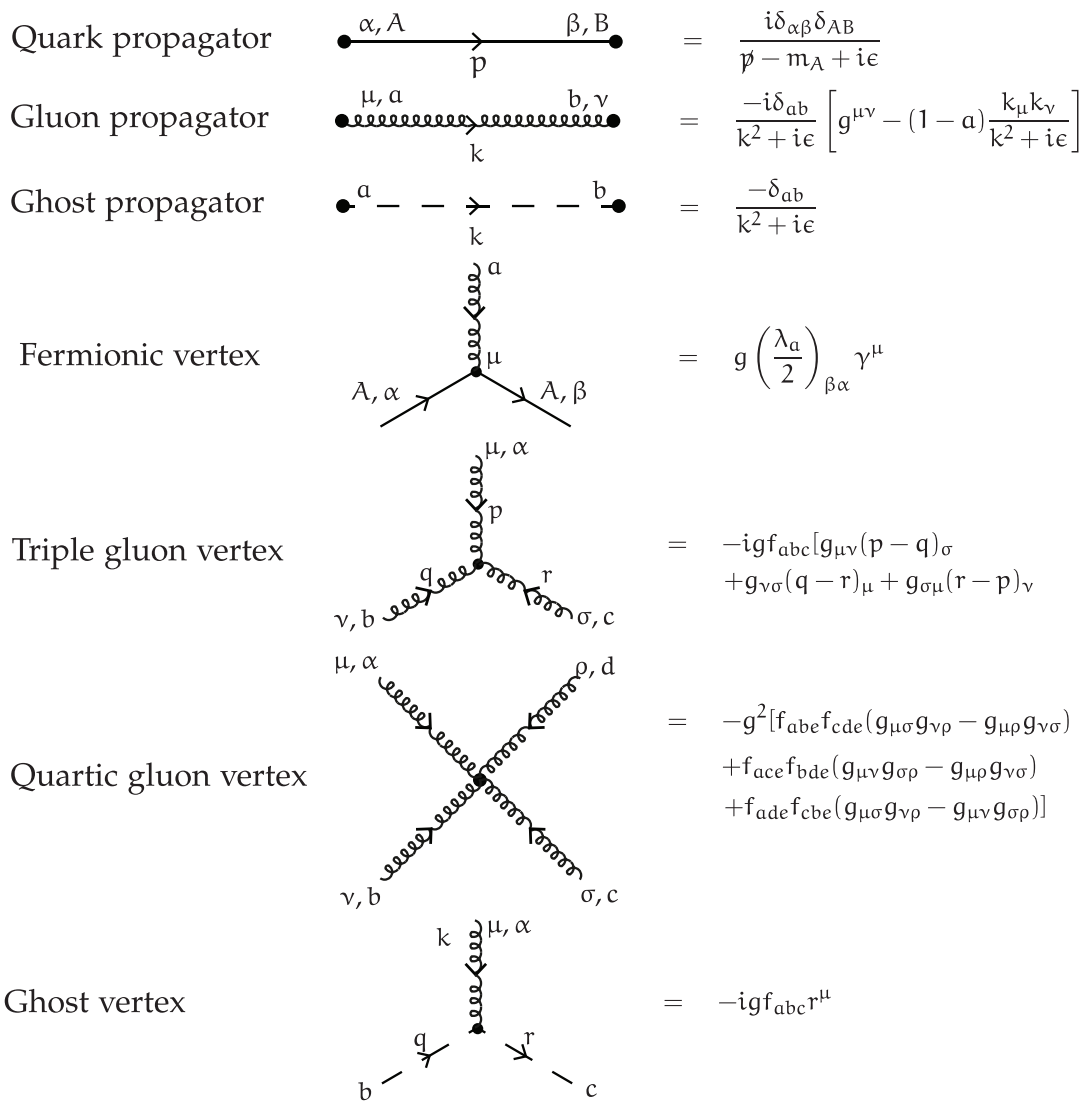

Figure 2.1: QCD Feynman rules.

The rest of the terms are the interaction terms. The fifth term represents the interaction between quarks and gluons and the last two terms the self-interactions of gluon fields.

The corresponding Feynman rules have been displayed in fig. 2.1. The rules are based on PT, but can be enhanced with the QCD condensates, as we will see in the discussion of the OPE in section 2.3

Having derived the Lagrangian leaves us with its quantisation. The dirac-spinors can be quantised as in QED without any problems. The $\Psi(x)$ quantum

field can be written as:

$$\Psi(x) = \int \frac{d^3p}{(2\pi)^3 2E(\vec{p})} \sum_\lambda \left[u(\vec{p},\lambda) a(\vec{p},\lambda) e^{-ipx} + v(\vec{p},\lambda) b^\dagger(\vec{p},\lambda) e^{ipx} \right], \tag{2.1.6}$$

where the integration ranges over the positive sheet of the mass hyperboloid $\Omega_+(m) = \{p | p^2 = m^2, p^0 > 0\}$. The four spinors $u(\vec{p},\lambda)$ and $v(\vec{p},\lambda)$ are solutions to the dirac equations in momentum space

$$\begin{aligned} [\not{p} - m] u(\vec{p},\lambda) &= 0 \\ [\not{p} + m] v(\vec{p},\lambda) &= 0, \end{aligned} \tag{2.1.7}$$

with λ representing the helicity state of the spinors.

The quantisation of the gauge fields is more cumbersome. One is forced to introduce supplementary non-physical fields, the so-called Faddeev-Popov ghosts $c^a(x)$ [27], to cancel unphysical helicity degrees of freedom of the gluon fields.

The free propagators for the quark, the gluon and the ghost fields are then given by

$$\begin{aligned} iS^{(0)AB}_{\alpha\beta}(x-y) &\equiv \overbrace{q^A_\alpha(x)\overline{q}^{\,B}_{\,\beta}}(y) \equiv \langle 0|T\{q^A_\alpha(x)\overline{q}^{\,B}_{\,\beta}\}|0\rangle = \delta_{AB}\delta_{\alpha\beta} iS^{(0)}(x-y) \\ &= i\delta_{AB}\delta_{\alpha\beta} \int \frac{d^4p}{(2\pi)^4} \frac{\not{p} + m}{(p^2 - m^2 + i\epsilon)} \\ iD^{(0)\mu\nu}_{ab}(x-y) &\equiv \overbrace{B^\mu_a(x)B^\nu_b}(y) \equiv \langle 0|T\{B^\mu_a(x)B^\nu_b(y)\}|0\rangle \equiv \delta_{ab} i \int \frac{d^4k}{(2\pi)^4} D^{(0)\mu\nu}(k) e^{-ik(x-y)} \\ &= i\delta_{ab} \int \frac{d^4k}{(2\pi)^4} \frac{1}{k^2 + i\epsilon} \left[-g_{\mu\nu} + (1-a)\frac{k_\mu k_\nu}{k^2 + i\epsilon} \right] e^{-ik(x-y)} \\ i\widetilde{D}^{(0)}_{ab}(x-y) &\equiv \overbrace{\phi_a(x)\overline{\phi}_{\,b}}(y) \equiv \langle 0|T\{\phi_a(x)\overline{\phi}_{\,b}(y)\}|0\rangle = \frac{i}{(2\pi)^4}\delta_{ab} \int d^4q \frac{-1}{q^2 + i\epsilon} e^{-q(x-y)} \\ &\equiv \frac{i}{(2\pi)^4}\delta_{ab} \int d^4q \widetilde{D}^{(0)}(q) e^{-iq(x-y)}, \end{aligned} \tag{2.1.8}$$

The previously introduced Feynman rules and propagators all make use of the perturbative vacuum $|0\rangle$ and are thus counted as tools of PT. Consequently they need a small coupling to approximate excitations the full QCD vacuum. We will see in the following section, that the strong coupling runs with energy and unfortunately is large for small energy scales.

2.1.1 Renormalisation Group

Computing observables with the QCD Lagrangian (eq. 2.1.3) lead to divergencies, which have to be *renormalised*. To render these divergent quantities finite we have to introducing a suitable parameter such that the "original divergent theory" corresponds to a certain value of that parameter. These procedure is referred to as *regularisation* and there are various approaches:

- **Cut-off regularisation:** In cut-off regularisation we limit the divergent momentum integrals by a cut-off $|\vec{p}| < \Lambda$. Here Λ has the dimension of mass. The cut-off regularisation breaks translational invariance, which can be guarded by making use of other regularisation methods.

- ***P-V* (Pauli-Villars) regularisation:** [44] In P-V regularisation the propagator is forced to decrease faster than the divergence to appear. It replaces the nominator by

$$(\vec{p}^2 + m^2)^{-1} \to (\vec{p}^2 + m^2)^{-1} - (\vec{p}^2 + M^2)^{-1}, \tag{2.1.9}$$

  where M has the dimension acts similar as the previously presented cut-off, but conserves translational invariance.

- **Dimensional regularisation:** [11, 2, 1] Dimensional regularisation has been introduced in the beginning of the seventies to regularise non-abelian gauge theories (like QCD), where Λ-and P-V-regularisation failed. In dimensional regularisation we expand the four space-time dimensions to arbitrary D-dimensions. To compensate for the additional dimensions we introduce an additional scale μ^{D-4}. A typical Feynman-integral then has the following appearance:

$$\int \frac{d^4 p}{(2\pi)^4} \frac{1}{\vec{p}^2 + m^2} \to \mu^{2\epsilon} \int \frac{d^D p}{(2\pi)^D} \frac{1}{\vec{p}^2 + m^2}, \tag{2.1.10}$$

  Dimensional regularisation preserves all symmetries, it allows an easy identification of divergences and naturally leads to the *minimal subtraction scheme* (MS) [1, 61].

In all of the three regularisation schemes we introduced an arbitrary parameter to regularise the divergence. This parameter causes scale dependence of the

strong coupling and the quark masses. As we are mainly concerned with the non-abelian gauge theory QCD we will focus on dimensional regularisation, which introduced the parameter μ. Measurable observables (*Physical quantities*) cannot depend on the renormalisation scale μ. Therefore the derivative by μ of a general physical quantity has to yield zero. A physical quantity $R(q, a_s, m)$, that depends on the external momentum q, the renormalised coupling $a_s \equiv \alpha_s/\pi$ and the renormalised quark mass m can then be expressed as

$$\mu\frac{d}{d\mu}R(q, a_s, m) = \left[\mu\frac{\partial}{\partial\mu} + \mu\frac{da_s}{d\mu}\frac{\partial}{\partial m} + \mu\frac{dm}{d\mu}\frac{\partial}{\partial m}\right] R(q, a_s, m) = 0. \tag{2.1.11}$$

Equation 2.1.11 is referred to as a *renormalisation group equation* (RGE) and is the basis for defining the two *renormalisation group functions*:

$$\beta(a_s) \equiv -\mu\frac{da_s}{d\mu} = \beta_1 a_s^2 + \beta_2 a_s^3 + \dots \qquad \beta - \text{function} \tag{2.1.12}$$

$$\gamma(a_s) \equiv -\frac{\mu}{m}\frac{dm}{d\mu} = \gamma_1 a_s + \gamma_2 a_s^2 + \dots \qquad \text{anomalous mass dimension.} \tag{2.1.13}$$

The β-function dictates the running of the strong coupling, whereas the anomalous mass dimension describes the running of the quark masses. We have a special interest in the running of the strong coupling, but will also shortly sum up the running of the quark masses.

Running gauge coupling

Regarding the β-function we notice, that $a_s(\mu)$ is not a constant, but that it *runs* by varying its scale μ. To better understand the running of the strong coupling we integrate the β-function

$$\int_{a_s(\mu_1)}^{a_s(\mu_2)} \frac{da_s}{\beta(a_s)} = -\int_{\mu_1}^{\mu_2} \frac{d\mu}{\mu} = \log\frac{\mu_1}{\mu_2}. \tag{2.1.14}$$

To analytically evaluate the above integral we can approximate the β-function to first order, with the known coefficient

$$\beta_1 = \frac{1}{6}(11N_c - 2N_f), \tag{2.1.15}$$

yielding

$$a_s(\mu_2) = \frac{a_s(\mu_1)}{\left(1 - a_s(\mu_1)\beta_1 \log\frac{\mu_1}{\mu_2}\right)}. \tag{2.1.16}$$

Equation 2.1.16 has some important implications for the strong coupling:

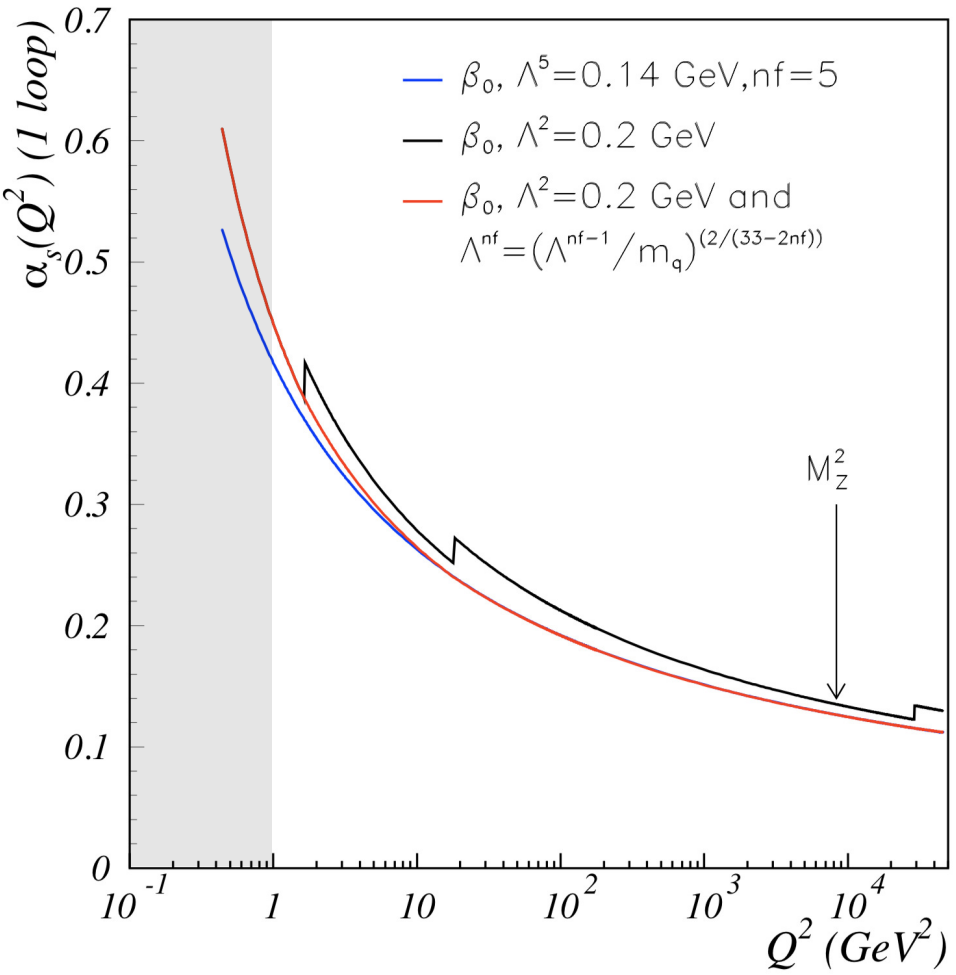

Figure 2.2: Running of the strong coupling $\alpha_s(Q^2)$ at first order. The blue line represents the uncorrected coupling constant, with an $\Lambda^{nf=5}$ chosen to match an experimental value of the coupling at $Q^2 = M_Z^2$. The quark-thresholds are shown by the black line and the corrected running is given by the red line. We additionally marked the breakdown of pt with a grey background for $Q^2 < 1$. The image is taken from an recent review of the strong coupling [24].

- The coupling at a scale μ_2 depends on $\alpha_s(\mu_1)$. Thus we have to take care of the scale μ, while comparing different values of α_s. In the literature (e.g. [**pdg2016**]) α_s is commonly compared at the Z-boson scale of around 91 GeV. As we are extracting the strong coupling at the mass of the tau lepton, around 1.776 GeV we need to run the strong coupling up to the desired scale. While running the coupling, we have to take care of the quark-thresholds. Each quark gets active at a certain energy scale, which leads to a running of α_s as shown in fig. 2.2. Typically one runs the coupling with the aid of software packages like *RunDec* [18, 32], which has also been ported to support C (*CRunDec*, [52]) and Python [57].

- As we have three colours ($N_c = 3$ and six flavours ($N_f = 6$ the first β_1 coefficient 2.1.12 is positive. Thus for $\mu_2 < \mu_1$ $\alpha_s(\mu_2)$ increases logarithmically and at a scale of $\mu_2 = 1$ GeV reaches a value of

$$\alpha_s(1\,\text{GeV}) \approx 0.5, \tag{2.1.17}$$

  which questions the applicability of PT for energies lower than 1 GeV (as seen from the grey zone in fig. 2.2).

- A large coupling for small scales implies confinement. We are not able to separate quarks in a meson or baryon. No quark has been detected as single particle yet. This is qualitatively explained with the gluon field carrying colour charge. These gluons form so-called *flux-tubes* between quarks, which cause a constant strong force between particles regardless of their separation. Consequently the energy needed to separate quarks is proportional to the distance between them and at some point there is enough energy to favour the creation of a new quark pair. Thus before separating two quarks we create a quark-antiquark pair. As a result we will probably never be able to observe an isolated quark. This phenomenon is referred to as colour confinement or simply confinement.

- With the first $\texttt{beta}_1$ coefficient being positive we notice that for increasing scales ($\mu_2 > \mu_1$) the coupling decreases logarithmically. This leads to asymptotic freedom, which states, that for high energies (small distances), the strong coupling becomes diminishing small and quarks and gluons do not interact. Thus in isolated baryons and mesons the quarks are separated by small distances, move freely and do not interact.

From the RGE we have seen, that not only the coupling but also the masses carry an energy dependencies.

Running quark mass

The mass dependence on energy is governed by the *anomalous mass dimension* $\gamma(a_s)$. Its properties of the running quark mass can be derived similar to the gauge coupling. Starting from integrating the *anomalous mass dimension* eq. 2.1.13

$$\log \frac{m(\mu_2)}{m(\mu_1)} = \int_{a_s(\mu_1)}^{a_s(\mu_2)} da_s \frac{\gamma(a_s)}{\beta(a_s)} \tag{2.1.18}$$

we can approximate the *anomalous mass dimension* to first order and solve the integral analytically [53]

$$m(\mu_2) = m(\mu_1) \left(\frac{a(\mu_2)}{a(\mu_1)}\right)^{\frac{\gamma_1}{\beta_1}} \left(1 + \mathcal{O}(\beta_2, \gamma_2)\right). \tag{2.1.19}$$

As β_1 and γ_1 (see 6.2) are positive the quark mass decreases with increasing μ. The general relation between different scales is given by

$$m(\mu_2) = m(\mu_1) \exp\left(\int_{a_s(\mu_1)}^{a_s(\mu_2)} da_s \frac{\gamma(a_s)}{\beta(a_s)}\right) \tag{2.1.20}$$

and can be solved numerically to run the quark mass to the needed scale μ_2. Both, the β-function and the anomalous mass dimension are currently known up to the 5^{th} order and listed in the appendix 6.1.

QCD in general has a precision problem caused by uncertainties and largeness of the strong coupling constant α_s. The fine-structure constant (the coupling QED) is known to eleven digits, whereas the strong coupling is only known to about four. Furthermore for low energies the strong coupling constant is much larger than the fine-structure constant. E.g. at the Z-mass, the standard mass to compare the strong coupling, we have an α_s of 0.11, whereas the fine structure constant would be around 0.007. Consequently to use PT we have to calculate our results to much higher orders, including tens of thousands of Feynman diagrams, in QCD to achieve a precision equal to QED. For even lower energies, around 1 GeV, the strong coupling reaches a critical value of around 0.5 leading to a break down of PT.

In this work we try to achieve a higher precision in the value of α_s. The framework we use to measure the strong coupling constant are the QCDSR. A central object needed to describe hadronic states with the help of QCD is the *two-point function* for which we will devote the following section.

2.2 Two-Point function

A lot of particle physics is dedicated to calculating the *S-matrix*, which contains all the information about how initial states evolve in time. One important tool for obtaining the S-matrix is the *LSZ (Lehmann-Symanzik-Zimmermann)-reduction formula* [41, 54]

$$\begin{aligned}\langle f|S|i\rangle = \left[i\int_0^\infty \frac{d^4x_1}{(2\pi)^4} e^{-ip_1x_1}(\Box^2+m^2)\right]\cdots\left[i\int_0^\infty \frac{d^4x_n}{(2\pi)^4} e^{ip_nx_n}(\Box^2+m^2)\right] \\ \times\langle\Omega|T\{\phi(x_1)\cdots\phi(x_n)\}|\Omega\rangle,\end{aligned} \tag{2.2.1}$$

with the $-i$ in the exponent applying for initial states and the $+i$ for final states. The LSZ-reduction formula relates the S-matrix to the *correlator* (also referred to as *n-point function*)

$$\langle\Omega|T\{\phi(x_1)\phi(x_2)\cdots\phi(x_n)\}|\Omega\rangle, \tag{2.2.2}$$

where $T\{\cdots\}$ is the time-ordered product and $|\Omega\rangle$ is the ground state/ vacuum of the interacting theory. Note that the fields are in general given in the Heisenberg picture, which implies translational invariance.

$$\begin{aligned}\langle\Omega|\phi(x)\phi(y)|\Omega\rangle &= \langle\Omega|\phi(x)e^{i\hat{P}y}e^{-i\hat{P}y}\phi(y)e^{i\hat{P}y}e^{-i\hat{P}y}|\Omega\rangle \\ &= \langle\Omega|\phi(x-y)\phi(0)|\Omega\rangle,\end{aligned} \tag{2.2.3}$$

where we made use of the translation operator $\hat{T}(x) = e^{-i\hat{P}x}$.

In this work we are solely concerned about the *two-point function*, especially in the vacuum expectation value of the Fourier transform of two time-ordered QCD quark Noether currents

$$\Pi_{\mu\nu}(q^2) \equiv \int \frac{d^4q}{(2\pi)^4} e^{iqx}\langle\Omega|J_\mu(x)J_\nu(0)|\Omega\rangle, \tag{2.2.4}$$

where the Noether current is given by

$$J_\mu(x) = \overline{q}(x)\Gamma q(x). \tag{2.2.5}$$

Here, Γ can be any of the following dirac matrices $\Gamma \in \{1, i\gamma_5, \gamma_\mu, \gamma_\mu\gamma_5\}$, specifying the quantum number of the current (S: *scalar*, P: *pseudo-Scalar*, V: *vectorial*, A: *axial-vectorial*, respectively). By choosing the right quantum numbers we can theoretically represent the processes we want to study, which will be important when we want to theoretically describe the hadrons produced in τ-decays.

From a Feynman diagram point of view we can illustrate the two-point function as quark-antiquark pair, which is produced by an external source, e.g. the virtual *W*-boson of $\tau\overline{\tau}$-annihilation as seen in fig. 2.3. Here the quarks are propagating at *short-distances*, which implies that we can make use of PT, thus avoiding *long-distance* (NPT-) effects, that would appear if the initial and final states where given by hadrons [19]. It is interesting to note, that the same process with the help of the *optical theorem* can be used to derive the total decay width of hadronic tau decays.

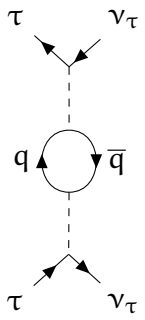

Figure 2.3: $\tau\overline{\tau}$-annihilation with a quark-antiquark pair.

2.2.1 Short-Distances vs. Long-Distances

If we want to calculate the two-point function in QCD we have to differentiate short-and long-distances or large or small momenta. In general when we talk about small distances we refer to large momenta. Large momenta implies a small strong coupling constant. Consequently we can use PT for short-distances without problems. On the contrary long distances involve small momenta, which implies a large coupling constant. Thus for long distances the NP effects become important and have to be dealt with. To apply PT to the case of the $\tau\overline{\tau}$ annihilation we need the quark-antiquark pair of **??** to be highly virtual [1]. To roughly separate long-distances from short-distances using a length scale we can say that the length scale should be smaller than the radius of a hadron.

[1] Which is the same of saying, that the quark-antiquark pair needs a high external momentum q.

Symbol	Quark content	Isospin	J	Current
π^0	$\frac{u\bar{u}-d\bar{d}}{2}$	1	0	$\bar{u}\gamma_\mu\gamma_5 u + \bar{d}\gamma_\mu\gamma_5 d$
η	$\frac{u\bar{u}+d\bar{d}-2s\bar{s}}{\sqrt{6}}$	0	0	$\bar{u}\gamma_\mu\gamma_5 u + \bar{d}\gamma_\mu\gamma_5 d - 2\bar{s}\gamma_\mu\gamma_5 s$
η'	$\frac{u\bar{u}+d\bar{d}+s\bar{s}}{\sqrt{3}}$	0	0	$\bar{u}\gamma_\mu\gamma_5 u + \bar{d}\gamma_\mu\gamma_5 d + \bar{s}\gamma_\mu\gamma_5 s$
ρ^0	$\frac{u\bar{u}-d\bar{d}}{\sqrt{2}}$	1	1	$\bar{u}\gamma_\mu u - \bar{d}\gamma_\mu d$
ω	$\frac{u\bar{u}+d\bar{d}}{\sqrt{2}}$	0	1	$\bar{u}\gamma_\mu u + \bar{d}\gamma_\mu d$
ϕ	$s\bar{s}$	0	1	$\bar{s}\gamma_\mu\gamma_5 s$

Table 2.2: Ground-state vector and pseudoscalar mesons for the light-quarks u, d and s with their corresponding currents in the two-point function. Note that we use γ_μ for vector and $\gamma_\mu\gamma_5$ for the pseudoscalar mesons.

2.2.2 Relating Two-Point Function and Hadrons

The two-point function can be interpreted physically as the amplitude of propagating single- or multi-particle states and their excitations. The possible states, in our case, the hadrons we describe through the correlator are fixed by the quantum numbers of the current we define for the vacuum expectation value. For example the neutral ρ-meson is a spin-1 vector meson with a quark content of $(u\bar{u} - d\bar{d})/\sqrt{2}$. Consequently by choosing a current

$$J_\mu(x) = \frac{1}{2}(\bar{u}(x)\gamma_\mu u(x) - \bar{d}(x)\gamma_\mu d(x)) \tag{2.2.6}$$

the two-point function contains the same quantum numbers as the ρ-meson and is said to materialise to it. A list of some ground-state mesons for combinations of the light quarks u, d and s is given in table 2.2.

The correlator is materialising into a spectrum of hadrons. Thus if we insert a complete set of states of hadrons we can make use of the unitary relation

$$\langle\Omega|J_\mu(x)_\nu(0)|\Omega\rangle = \sum_X \langle\Omega|J_\mu(x)|X\rangle\langle X|J_\nu(0)|\Omega\rangle. \tag{2.2.7}$$

to represent the two-point correlator via a spectral function $\rho(t)$

$$\Pi(q^2) = \int_0^\infty ds \frac{\rho(s)}{s - p^2 - i\epsilon}. \tag{2.2.8}$$

The above relation is referred to as *Källén-Lehmann spectral representation* [36, 40] or *dispersion relation*. It relates the two-point function to the spectral function

ρ, which can be represented as sum over all possible hadronic states

$$\rho(s) = (2\pi)^3 \sum_X \int \left|\langle \Omega | J_\mu(0) | X \rangle\right|^2 \delta^4(s - p_X). \tag{2.2.9}$$

Note that the analytic properties of the two-point are in one-to-one correspondence with the newly introduced spectral function and thus determined by the possible hadrons states, which only form on the positive real axis. A full derivation of the *Källén-Lehmann spectral representation* can be found in the appendix chapter 7. We will derive the same representation to a later point by solely using the analytic properties of the correlator (see. section 2.4). The spectral function is interesting to us for two reasons. First it is experimentally measurable and second it carries a problematic "branch cut", which we want to discuss now.

2.2.3 Analytic Structure of the Two-Point Function

The general two-point function $\rho(s)$ has some interesting, but problematic analytic properties. It has poles for single-particle states and a continuous branch cut for multi-particle states. The single and multi-particle states, for a general correlator, can be mathematically separated by

$$\rho(s) = Z\delta(s - m^2) + \theta(s - s_0)\sigma(s) + \sigma(s), \tag{2.2.10}$$

where the second term is the contribution from multi-particle states. $\sigma(s)$ is zero till we reach the threshold, where we have sufficient energy to form multi-particle states. The analytic structure is depicted by fig. 2.4 and we can see that the spectral function has δ-spikes for single-particle states and a continuous contribution for $s \geqslant 4m$ resulting from multi-particle states. These lead to poles and a continuous branch cut of the two-point function.

2.2.4 Lorentz Decomposition

Apart the spectral decomposition we can Lorentz decompose the correlator to a scalar function $\Pi(q^2)$. Due to Lorentz invariance, there exist only two possible terms that can guard the structure of the second order tensor: $q_\mu q_\nu$

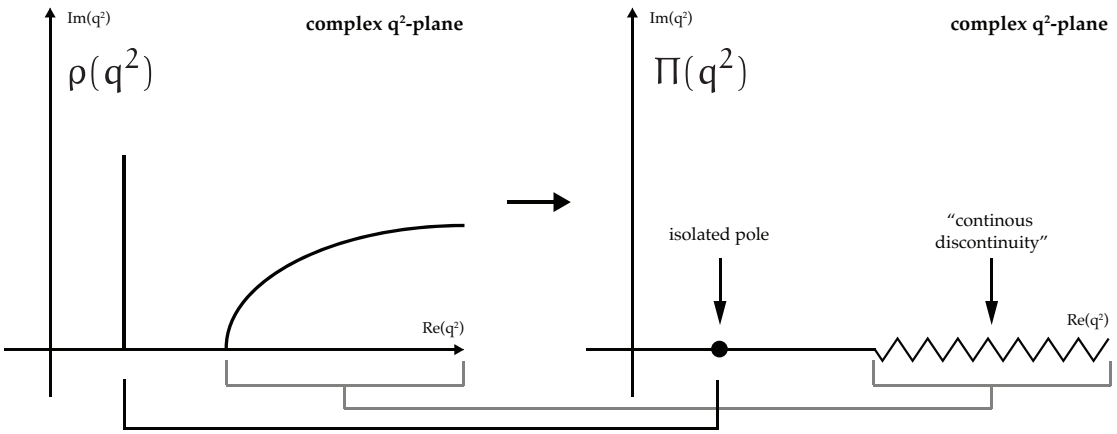

Figure 2.4: Analytic structure in the complex q^2-plane of the Fourier transform of the two-point function. The hadronic final states are responsible for poles appearing on the real-axis. The one-particle states contribute as isolated pole and the multi-particle states contribute as bound-states poles or a continues "discontinuity cut" [45, 68].

and $q^2 g_{\mu\nu}$. The sum of both multiplied with two arbitrary functions $A(q^2)$ and $B(q^2)$ yields

$$\Pi_{\mu\nu}(q^2) = q_\mu q_\nu A(q^2) + q^2 g_{\mu\nu} B(q^2). \tag{2.2.11}$$

By making use of the *Ward-identity*

$$q^\mu \Pi_{\mu\nu} = 0 \tag{2.2.12}$$

The Ward identity is dependent on the conserved Noether-current J_μ and thus only holds for same flavour quarks. With the Ward-identity we are able to demonstrate, that the two arbitrary functions are related

$$\begin{aligned} q^\mu q^\nu \Pi_{\mu\nu} = q^4 A(q^2) + q^4 B(q^2) = 0 \\ \implies A(q^2) = -B(q^2). \end{aligned} \tag{2.2.13}$$

Thus redefining $A(q^2) \equiv \Pi(q^2)$ we expressed the correlator as a scalar function

$$\Pi_{\mu\nu}(q^2) = (q_\mu q_\nu - q^2 g_{\mu\nu}) \Pi(q^2). \tag{2.2.14}$$

2.2.5 More Decompositions

compositions check! The two-point function can be Lorentz decomposed, but we can also decompose it into its transversal and longitudinal components.

Both, the longitudinal and transversal components are related and have implications for a common used approximation: the **chiral limit**, where the quark masses are taken to zero ($m_q \to 0$).

Starting with the decomposition into *vector* (V), *axial-vector* (A), *scalar* (S) and *pseudo-scalar* (P) components we can write [13, 35]

$$\begin{aligned}\Pi^{\mu\nu}(q^2) = (q^\mu q^\nu - q^2 g^{\mu\nu})\Pi^{V,A}(q^2) + \frac{g^{\mu\nu}}{q^2}(m_i \mp m_j)\Pi^{S,P}(q^2) \\ + g^{\mu\nu}\frac{(m_i \mp m_j)}{q^2}[\langle\Omega|\overline{q}_i q_i|\Omega\rangle \mp \langle\Omega|\overline{q}_j q_j|\Omega\rangle],\end{aligned} \tag{2.2.15}$$

which is composed of a vector $\Pi^{V,A}$ and scalar $\Pi^{S,P}$ part. The third term is a correction arising due to the physical vacuum $|\Omega\rangle$. The latter decomposition rewrites the correlator $\Pi^{\mu\nu}(q^2)$ into transversal and longitudinal components:

$$\Pi^{\mu\nu}(q^2) = (q^\mu q^\nu - g^{\mu\nu}q^2)\Pi^{(T)}(q^2) + q^\mu q^\nu \Pi^{(L)}(q^2). \tag{2.2.16}$$

With the two decompositions eq. 2.2.15 and eq. 2.2.16 we can now identify the longitudinal components of the correlator as being purely scalar, by multiplying eq. 2.2.15 by two four-momenta and making use of the Ward-idendity eq. 2.2.12 we can write

$$q_\mu q_\nu \Pi^{\mu\nu}(q^2) = (m_i \mp m_j)^2 \Pi^{S,P}(q^2) + (m_i \mp m_j)[\langle\overline{q}_i q_i\rangle \mp \langle\overline{q}_j q_j\rangle], \tag{2.2.17}$$

which then can be related to the longitudinal component of eq. 2.2.16 by comparison of the two equations

$$q_\mu q_\nu \Pi^{\mu\nu}(q^2) = q^4 \Pi^{(L)}(q^2) = s^2 \Pi^{(L)}(s) \quad \text{with} \quad s \equiv q^2. \tag{2.2.18}$$

In a more eloquent way this can be expressed as

$$s^2 \Pi^{(L)}(s) = (m_i \mp m_j)^2 \Pi^{(S,P)}(s) + (m_i \mp m_j)[\langle\overline{q}_i q_i\rangle \mp \langle\overline{q}_j q_j\rangle], \tag{2.2.19}$$

where we can see, that all mass terms are related to the longitudinal component of the correlator.

We note, that the longitudinal component in **??** and the scalar component in eq. 2.2.15 vanish in the chiral limit, which will become handy in the next chapter.

By defining a combination of the transversal and longitudinal correlator

$$\Pi^{(T+L)}(s) \equiv \Pi^{(T)}(s) + \Pi^{(L)}(s) \tag{2.2.20}$$

we can additionally relate the transversal and vectorial components via

$$\Pi^{\mu\nu}(s) = \underbrace{(q^\mu q^\nu - g^{\mu\nu}q^2)\Pi^{(T)}(s) + (q^\mu q^\nu - g^{\mu\nu}q^2)\Pi^{(L)}(s)}_{=(q^\mu q^\nu - g^{\mu\nu}q^2)\Pi^{(T+L)}(s)} + \frac{g^{\mu\nu}s^2}{q^2}\Pi^{(L)}(s), \quad (2.2.21)$$

such that

$$\Pi^{(V,A)}(s) = \Pi^{(T)}(s) + \Pi^{(L)} = \Pi^{(T+L)}, \quad (2.2.22)$$

where the vector/ axial-vector component of the correlator is now related to the newly defined transversal and longitudinal combination of the correlator. As the tau decays, with the limiting factor of the tau mass, can only decay into light quarks we will often neglect the quark masses and work in the so called chiral limit. In the chiral limit the longitudinal component of the correlator, which is proportional to the quark masses, vanishes.

Having dealt exclusively with the perturbative part of the theory, we have to discuss NP contributions. These arise due to non negligible long-distance effects. Thus to complete the needed ingredients for *Sum Rules* we need a final ingredient the *Operator Product Expansion* (OPE), which treats the non-perturbative contributions of our theory.

2.3 Operator Product Expansion

The OPE was introduced by Wilson in 1969 [66] as an alternative to the in this time commonly used current-algebra. The expansion states that non-local operators can be rewritten into a sum of composite local operators and their corresponding coefficients:

$$\lim_{x\to y} A(x)B(y) = \sum_n C_n(x-y)\mathcal{O}_n(x), \quad (2.3.1)$$

where $C_n(x-y)$ are the so-called *Wilson-coefficients* and A, B and $\mathcal{O}_n$ are operators.

The OPE lets us separate short distances from long distances. In pure PT we can only amount for short distances, which are equal to high energies, where the strong-coupling α_s is small. The OPE on the other hand accounts for long-distance effects with higher dimensional operators.

The form of the composite operators are dictated by gauge- and Lorentz symmetry. Thus we can only make use of operators of even dimension. The scalar operators up to dimension six are given by [43]

$$\begin{aligned}
&\text{Dimension 0:} && \mathbb{1} \\
&\text{Dimension 4:} && :m_i\overline{q}\,q: \\
& && :G_a^{\mu\nu}(x)G^a_{\mu\nu}(x): \\
&\text{Dimension 6:} && :\overline{q}\,\Gamma q\overline{q}\,\Gamma q: \\
& && :\overline{q}\,\Gamma\tfrac{\lambda^a}{2}q_\beta(x)\overline{q}\,\Gamma\tfrac{\lambda^a}{2}q: \\
& && :m_i\overline{q}\,\tfrac{\lambda^a}{2}\sigma_{\mu\nu}qG_a^{\mu\nu}: \\
& && :f_{abc}G_a^{\mu\nu}G_b^{\nu\delta}G_c^{\delta\mu}:,
\end{aligned} \tag{2.3.2}$$

where Γ stands for one of possible dirac matrices (as seen eq. 2.2.5). The operator of dimension zero is the identity and its Wilson-coefficient is solely perturbative. The higher dimension operators appear as normal ordered products of fields and vanish by being sandwiched into the perturbative vacuum. On the contrary, in NP QCD they appear as *condensates*. Condensates are the vacuum expectation values of non-vanishing normal ordered fields by applying the full QCD vacuum, which contribute to all strong processes. For example the condensates of dimension four are the quark-condensate $\langle\overline{q}\,q\rangle$ and the gluon-condensate $\langle GG\rangle$.

As we work with dimensionless functions (e.g. the correlator Π), the r.h.s. of eq. 2.3.1 has to be dimensionless. As a result the Wilson-coefficients have to cancel the dimension of the operator with their inverse mass dimension. To account for the dimensions we can make the inverse momenta explicit

$$\Pi^{\text{OPE}}_{V/A}(s) = \sum_{D=0,2,4\ldots} \frac{c^{(D)}\langle\mathcal{O}^{(D)}(x)\rangle}{(-q^2)^{D/2}}, \tag{2.3.3}$$

where we used $C^{(D)} = c/(-s)^{D/2}$ with D being the dimension. Thus the OPE should converge with increasing dimension for sufficiently large momenta s.

2.3.1 A practical example

Let's show how the OPE contributions are calculated [56, 43]. We will compute the perturbative and quark-condensate Wilson-coefficients for the rho meson. To do so we have to evaluate Feynman diagrams using standard PT.

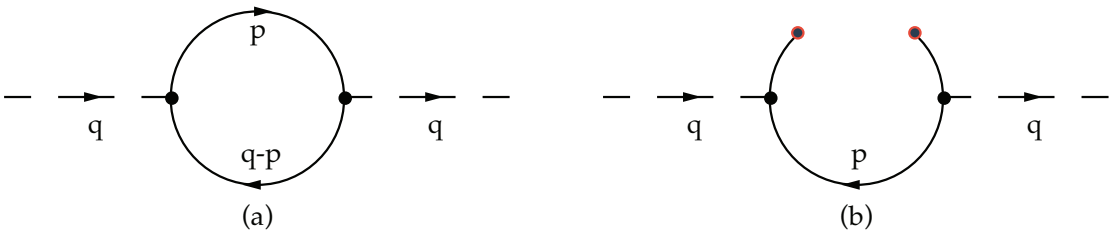

Figure 2.5: Feynman diagrams of the perturbative (a) and the quark-condensate (b) contribution. The upper part of the right diagram is not wick-contracted and responsible for the condensate.

The rho meson is a vector meson of isospin one composed of u and d quarks. As a result (see. table 2.2) we can match its quantum numbers with the current

$$J^{\mu}(x) = \frac{1}{2}\left(:[\overline{u}\,\gamma^{\mu}u](x) - [\overline{d}\,\gamma^{\mu}d](x):\right). \tag{2.3.4}$$

Pictorial the dimension zero contribution is given by the quark-antiquark loop Feynman diagram fig. 2.5. The higher dimension contributions are given by the same Feynman diagram, but with non contracted fields. These non contracted fields contain the condensates. Thus not contracting the quark-antiquark field (see. fig. 2.5 b) will give us access to the Wilson coefficient of the dimension four quark-condensate $\langle\overline{q}\,q\rangle$.

The perturbative part (the Wilson coefficient of dimension zero) can than be taken from the mathematical expression for the scalar correlator

$$\begin{aligned}\Pi(q^2) = -\frac{i}{4q^2(D-1)}\int d^D x e^{iqx}\langle\Omega|T\{:\overline{u}\,(x)\gamma^{\mu}u(x) - \overline{d}\,(x)\gamma^{\mu}d(x):\\ \times :\overline{u}\,(0\gamma_{\mu}u(0) - \overline{d}\,(0)\gamma_{\mu}d(0):\}\rangle.\end{aligned} \tag{2.3.5}$$

To extract the dimension zero Wilson coefficient we apply Wick's theorem to contract all of the fields, which represents the lowest order of the perturbative contribution. The calculation is only using standard PT and we will restrict ourselves in displaying the result and omitting the calculation[2].

$$\begin{aligned}\Pi(q^2) &= \frac{i}{4q^2(D-1)}(\gamma^{\mu})_{ij}(\gamma_{\mu})_{kl}\int d^D x e^{iqx}\\ &\times \quad \left[\overbrace{u_{j\alpha}(x)\overline{u}_{k\beta}}(0)\cdot\overbrace{u_{l\beta}(0)\overline{u}_{i\alpha}}(x) + (u\to d)\right]\\ &= \frac{3}{8\pi^2}\left[\frac{5}{3} - \log\left(-\frac{q^2}{\nu^2}\right)\right].\end{aligned} \tag{2.3.6}$$

[2]The interested reader can follow [43] for a detailed calculation.

To calculate the higher dimensional contributions of the OPE we use the same techniques as before, but leave some of the fields uncontracted. Thus instead of applying Wick's theorem for all possible contractions fields, we leave some fields uncontracted. For leaving the quark field uncontracted in eq. 2.3.5 we get

$$\begin{aligned}\Pi(q^2) = \frac{i}{4q^2(D-1)}(\gamma^\mu)_{ij}(\gamma_\mu)_{kl}\int d^D x e^{iqx}\Big[\\ + \overbrace{u_{j\alpha}(x)\bar{u}}_{k\beta}(0)\cdot\langle\Omega|:\bar{u}_{i\alpha}(x)u_{l\beta}(0):|\Omega\rangle \\ + \overbrace{u_{l\beta}(0)\bar{u}}_{i\alpha}(x)\cdot\langle\Omega|:\bar{u}_{k\beta}(0)u_{j\alpha}(x):|\Omega\rangle + (u\to d)\Big].\end{aligned} \tag{2.3.7}$$

Here we can observe the condensates as non-vanishing vacuum values of normal ordered product of fields:

$$\langle\Omega_{QCD}|\bar{q}(x)q(0)|\Omega_{QCD}\rangle \neq 0. \tag{2.3.8}$$

We emphasised the QCD vacuum Ω_{QCD}, which is responsible for vacuum expectation values different than zero. E.g. for a vacuum of QED this contributions would vanish by definition. Pictorial the condensates take form of unconnected propagators, sometimes marked with an x, as seen in fig. 2.5.

To make the non-contracted fields local, we can expanded them in x

$$\begin{aligned}\langle\Omega|:\bar{q}(x)q(0):|\Omega\rangle = \langle\Omega|:\bar{q}(0)q(0):|\Omega\rangle \\ + \langle\Omega|:\left[\partial_\mu\bar{q}(0)\right]q(0):|\Omega\rangle x^\mu + \dots.\end{aligned} \tag{2.3.9}$$

and introduce a standard notation for the localised condensate

$$\langle\bar{q}\,q\rangle \equiv \langle\Omega|:\bar{q}(0)q(0):|\Omega\rangle. \tag{2.3.10}$$

Finally, the contribution to the rho scalar correlator is then given by the following expression

$$\Pi_{(\rho)}(q^2) = \frac{1}{2}\frac{1}{(-q^2)^2}\left[m_u\langle\bar{u}\,u\rangle + m_d\langle\bar{d}\,d\rangle\right]. \tag{2.3.11}$$

Here we can clearly see that for dimension four we get a factor of $1/(-q^2)^2$, which is responsible for the suppression of the series. The condensates $\langle\bar{u}\,u\rangle$ and $\langle\bar{d}\,d\rangle$ are numbers, that have to be derived by phenomenological fits or LQCD. Fortunately once found, the value of the condensate can be used for any process.

In summary we note that the usage of the OPE and its validity is far from obvious. Until today there is no analytic proof of the OPE. Furthermore we are deriving the OPE from matching the Wilson-coefficients to Feynman-graph analyses. These Feynman-graphs are calculated perturbatively but the coefficients with dimension $D > 0$ correspond to NP condensates! The condensates by themselves have to be gathered from external, NP methods.

Now that we have a tool to deal with the problematic QCD vacuum and NPT-effects we are left with two problems. First we still do not know how to deal with hadronic states in the quark-gluon picture. This will be tackled by Duality. Secondly we have seen that we can access the two-point function theoretically on the physical sheet except for the positive real axis, due to its analytic properties. Unfortunately the experimental measurable spectral function is solely be defined on this positive real axis, which is theoretically not accessible. To match the theory with the experiment we will have to apply Cauchy's theorem. In the final section of this chapter we will bring together the two-point function, the OPE, Duality and Cauchy's theorem to formulate the QCDSR.

2.4 Sum Rules

The QCDSR are a method of QCD to bridge the fundamental degrees of QCD, in our case the strong coupling, to the observable spectrum of hadrons. To do so we have to treat the in section 2.2 introduced two-point function in non-perturbatively with the help of the OPE

$$\Pi(s) \to \Pi_{OPE}(s). \tag{2.4.1}$$

QCDSR furthermore introduce an ad hoc assumption, namely *quark-hadron duality*, of stating that the observable hadron picture can be equally described by the QCD quark-gluon picture. As the experimentally measured hadronic states are represented in poles and cuts on the positive real axis of the two-point function, which we have encountered in the analytic properties of its spectral decomposition, the QCDSR give us a description on how to apply *Cauchy's theorem* and weight functions to take care of perturbative complications close to the positive real axis.

2.4.1 The Dispersion Relation

We have already seen the Källén-Lehmann spectral representation in **??**. The general dispersion relation is defined to have an additional polynomial function $P(s)$

$$\Pi(s) = \int_0^\infty \frac{\rho(s')}{s' - s - i\epsilon} + P(s), \tag{2.4.2}$$

which accounts for fact, that the two-point function increases for large s, but the integral on the RHS cannot reproduce this behaviour. For example the vector correlator carries only a constant and the scalar correlator a linear polynom. The two-point function is in general an unphysical quantity, whereas the spectral function $\rho(s)$ is a physical quantity. As a result the polynomial accounts carries the unphysical scale dependency of the two-point function.

2.4.2 Duality

QCD treats quarks and gluon as its fundamental DOF, but due to confinement we are only ever able to observe hadrons. The mechanism that connects the two worlds is the *quark-hadron duality* (or simply duality), which implies that physical quantities can be described equally good in the hadronic or in the quark-gluon picture. Thus we can connect experimental detected with theoretically calculated values from the two-point function in the dispersion relation eq. 2.4.2 as

$$\Pi_{th}(s) = \int_0^\infty \frac{\rho(s')_{exp}}{s' - s - i\epsilon} + P(s), \tag{2.4.3}$$

where we connected the theoretical correlator Π_{th} with the experimental measurable spectral function ρ_{exp}. A detailed discussion of duality has been given by the author of the Shifman2000.

if time add duality violation paragraph

2.4.3 Finite Energy Sum Rules

To theoretical calculate the two-point function we have to integrate the experimental data $\rho_{exp}(s)$ to infinity. No experiment will ever take data for an infi-

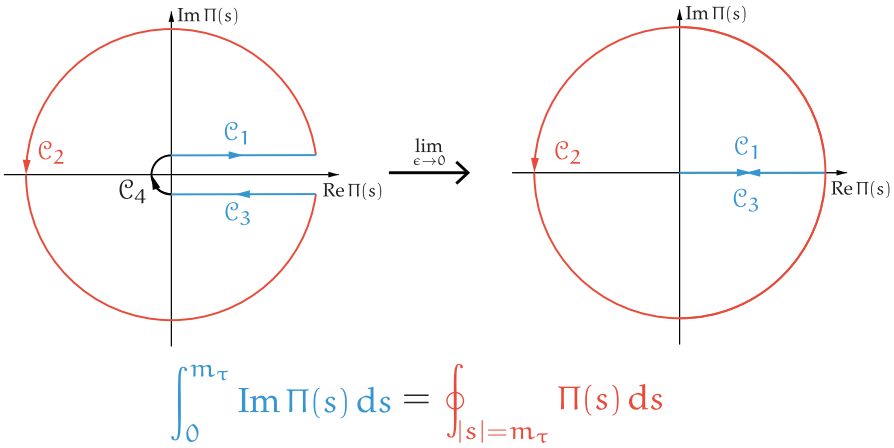

Figure 2.6: Visualisation of the usage of Cauchy's theorem to transform eq. 2.4.2 into a closed contour integral over a circle of radius s_0.

nite momentum s. For tau decays we are currently limited to energies around the tau-mass of $1.776\,GeV$. To deal with the upper integration limit several approaches have been made. One of them, the *Borel transformation* is to exponentially suppress higher energy contributions (see [64, 50]). The technique we are using is called *finite energy sum rules* (FESR) and introduces a energy cut-off. We thus integrate the experimental data $\rho(s)$ only to a certain energy s_0, like

$$\Pi(s) = \int_0^{s_0} \frac{\rho(s')}{s' - s - i\epsilon} + P(s). \tag{2.4.4}$$

Unfortunately we still cannot theoretically evaluate the *right-hand side* (RHS) as the line integral includes the singularities of the spectral function. As a result we have to apply Cauchy's theorem

$$\oint_{\mathcal{C}} f(z) = 0, \tag{2.4.5}$$

which states that any integral over an analytic function $f(z)$ on a closed contour $\mathcal{C}$ has to be zero. Thus we can construct a contour to avoid the positive problematic real axis. Pictorial the contour is drawn in fig. 2.6 and mathematically we can express it as

$$\oint \Pi(s) = \int_0^{s_0} \Pi(s + i\epsilon) - \Pi(s - i\epsilon)\,ds + \int_{0+\alpha(\epsilon)}^{2\pi-\alpha(\epsilon)} \Pi(s_0 e^{i\theta})\,d\theta + \int_{3\pi/2}^{\pi/2} \Pi(s_0 e^{i\theta})\,d\theta \tag{2.4.6}$$

If we make to use of *Schwartz reflection principle*:

$$f(\bar{z}) = \overline{f(z)}, \tag{2.4.7}$$

which can be applied if f is analytic and maps only to real values on the positive real axis, we can express the integrand of the first integral of eq. 2.4.6 as the imaginary part of the two-point function

$$\Pi(s+i\epsilon) - \Pi(s-i\epsilon) = \Pi(s+i\epsilon) - \Pi^*(s+i\epsilon) = 2i\,\mathrm{Im}\,\Pi(s+i\epsilon), \tag{2.4.8}$$

which is by definition equal to the spectral function

$$\rho(s) \equiv \frac{\Pi(s)}{\pi}. \tag{2.4.9}$$

After taking the limit of small epsilon we can relate the line integral to a finite momentum s0 experimental spectral function to a theoretical accessible circular contour integral of radius s_0

$$\int_0^{s_0} \rho(s) = \frac{-1}{2\pi i} \oint_{|s|=s_0} \Pi(s)\,ds, \quad \text{where we applied} \quad \epsilon \to 0. \tag{2.4.10}$$

Note that the unphysical of the polynomial in eq. 2.4.2 cancel in the contour integral.

We are free to multiply the upper equation with an analytic function $\omega(s)$, which completes the FESR

$$\int_0^{s_0} \omega(s)\rho(s) = \frac{-1}{2\pi i} \oint_{|s|=s_0} \omega(s)\Pi_{OPE}(s)\,ds \tag{2.4.11}$$

where the *left-hand side* (LHS) is given by the experiment and the RHS. can be theoretically evaluated by applying the OPE of the correlator $\Pi_{OPE}(s)$. The analytic function $\omega(s)$ plays the role of a weight. It can be used to further suppress the non-perturbative contributions coming from as *duality violations* and also enhance or suppress different contributions of the OPE as we will see.

2.4.4 Pinched weights to avoid DVs

We are free to multiply **??** by an analytic weight function $\omega(s)$

$$\int_0^{m_\tau} \omega(s)\Pi(s)\,ds = \frac{i}{2} \oint_{s=m_\tau} \omega(s)\Pi(s)\,ds. \tag{2.4.12}$$

We can use this technique to suppress contributions for the two-point function close to the positive real axis by implementing so called pinched weights of the form

$$\omega(s) = \left(1 - \frac{s}{m_\tau^2}\right)^k, \tag{2.4.13}$$

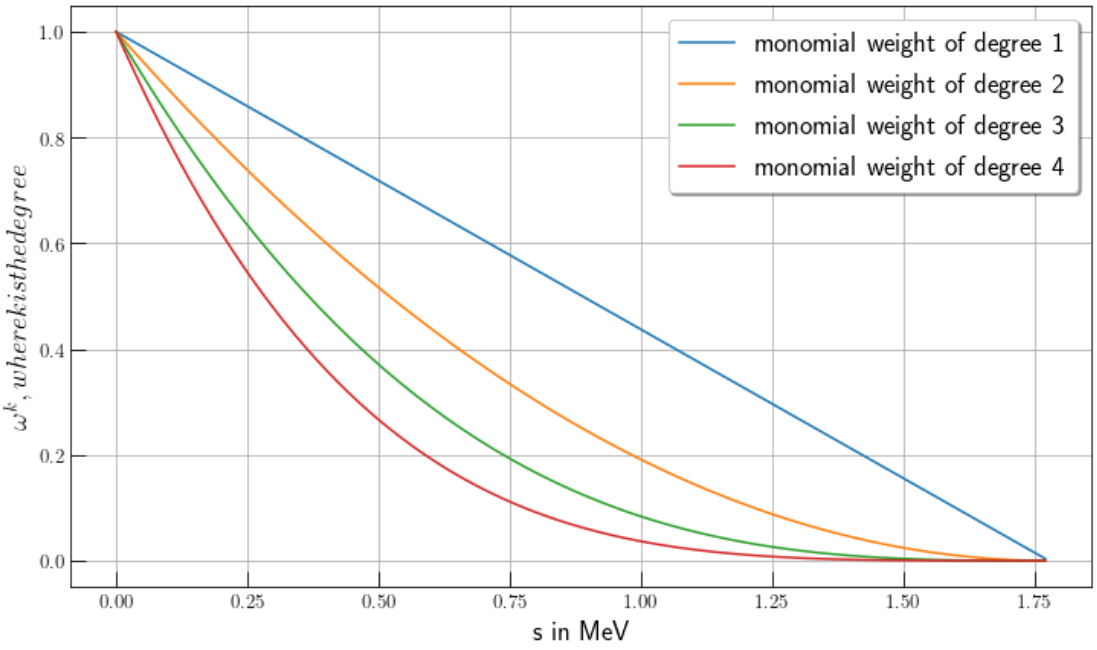

Figure 2.7: Monomial weights $(1 - s/m_\tau^2)^k$ for degrees $1 \to 4$. We can see that weights of higher pinching decrease faster, which comes in handy if we want to suppress duality violations.

where k is the degree of the pinched weight. The higher the degree the farther we operate from the critical positive real axis (see. **??**), which suppresses the effects of duality violations. This pinching of second degree appears quite naturally. If we regard the include $\tau - decay$ ratio eq. 3.1.5, we note that for the transversal component we already have a double pinched weight, the *kinematic weight*

$$\omega_\tau(s) = \left(1 - \frac{s}{m_\tau^2}\right)\left(1 + 2\frac{s}{m_\tau^2}\right). \tag{2.4.14}$$

In general it is said that a double pinched weight is sufficient to neglect effects caused by duality violation.

We can also use different weights to control the dimensions of the OPE that contribute. The weights we are using have to be analytic, so that we can make use of Cauchy's theorem. Thus they can be represented as polynomials

$$\omega(x) = \sum_i a_i x^i, \tag{2.4.15}$$

every contributing monomial is responsible for a dimension of the OPE. Dimensions that are not represented in the weight polynomial do not contribute at all or are very suppressed as we will demonstrate now.

monomial:	x^0	x^1	x^2	x^3	x^5	x^6	x^7
dimension:	$D^{(2)}$	$D^{(4)}$	$D^{(6)}$	$D^{(8)}$	$D^{(10)}$	$D^{(12)}$	$D^{(14)}$

Table 2.3: List of monomial and their corresponding "active" dimensions in the OPE.

The residue of a monomial x^k is only different from 0 if its power $k = -1$:

$$\oint_C x^k \, dx = i \int_0^{2\pi} \left(e^{i\theta}\right)^{k+1} d\theta = \begin{cases} 2\pi i & \text{if } k = -1, \\ 0 & \text{otherwise} \end{cases}. \tag{2.4.16}$$

Consequently if we exchange the kinematic weight of the include ratio eq. 3.1.1 through a monomial and neglect all terms of no interest to us we can write

$$\begin{aligned} R(xm_\tau)\big|_{D=0,2,4\ldots} &= \oint_{|x|=1} \frac{x^k}{(xm_\tau)^{\frac{D}{2}}} C^D(xm_\tau) \\ &= \frac{1}{(m_\tau)^{\frac{D}{2}}} \oint_{|x|=1} x^{k-D/2} \, C^D(xm_\tau), \end{aligned} \tag{2.4.17}$$

where C^D are the D-dimensional Wilson coefficients. Thus combining eq. 2.4.16 with eq. 2.4.17 we see that only Dimension which fulfill

$$k - D/2 = -1 \quad \Longrightarrow \quad D = 2(k+1) \tag{2.4.18}$$

contribute to the OPE. For example the polynomial of the kinematic weight is given by

$$(1-x)^2(1+2x) = \underbrace{1}_{D=2} - 3\underbrace{x^2}_{D=6} + 2\underbrace{x^3}_{D=8}, \tag{2.4.19}$$

where we underbraced the monomial and gave the active dimensions. A list of monomomials and their corresponding Dimensions up to dimension 14 can be found in table 2.3. This behavior enables us to bring out different dimensions of the OPE and suppress contributions of higher order ($D \geqslant 10$) for which less is known.

For the interested reader we gathered several introduction texts to the QCDSR, which where of great use to us [42, 50, 19, 26].

Chapter 3

Tau Decays into Hadrons

Building on the previously presented QCDSR we will elaborate the needed theory to extract α_s from the process of hadronic tau decays. ... complete

3.1 Tau Decays into hadrons

The tau lepton is the only lepton heavy enough to decay into hadrons. It permits one of the most precise determinations of the strong coupling α_s. The inclusive tau decay ratio

$$R_\tau = \frac{\Gamma(\tau \to \nu_\tau + \text{hadrons})}{\Gamma(\tau \to \nu_\tau e^+ e^-)} \tag{3.1.1}$$

can be precisely calculated and is sensitive to α_s. Due to the small mass of the tau lepton $m_\tau \approx 1.776\,\text{GeV}$ the tau decays are excellent for performing a low-energy QCD analysis. The theoretical expression of the hadronic tau decay ratio was first derived by [60], using current algebra, a more recent derivation making use of the *optical theorem*, as already mentioned in section 2.2 can be taken from [53].

3.1.1 The Inclusive Decay Ratio

The inclusive ratio is given by:

$$R_\tau(s) = 12\pi \int_0^{m_\tau} \frac{ds}{m_\tau^2} \left(1 - \frac{s}{m_\tau^2}\right) \left[\left(1 + 2\frac{s}{m_\tau^2}\right) \operatorname{Im}\Pi^{(T)}(s) + \operatorname{Im}\Pi^{(L)}(s)\right], \tag{3.1.2}$$

where $\mathrm{Im}\,\Pi$ is imaginary part of the two-point function we introduced in section 2.2. Applying Cauchy's theorem, as seen in **??**, to the eq. 3.1.2 we get

$$R_\tau = 6\pi i \oint_{s=m_\tau} \frac{ds}{m_\tau^2}\left(1-\frac{s}{m_\tau^2}\right)\left[\left(1+2\frac{s}{m_\tau^2}\right)\Pi^{(T)}(s)+\Pi^{(L)}(s)\right]. \tag{3.1.3}$$

It is furthermore convenient to work with $\Pi^{(T+L)}$, which has been defined in eq. 2.2.20. As a result we can further rewrite the hadronic tau decay ratio into

$$R_\tau = 6\pi i \oint_{|s|=m_\tau} \frac{ds}{m_\tau^2}\left(1-\frac{s}{m_\tau^2}\right)^2\left[\left(1+2\frac{s}{m_\tau^2}\right)\Pi^{(L+T)}(s)-\left(\frac{2s}{m_\tau^2}\right)\Pi^{(L)}(s)\right]. \tag{3.1.4}$$

In the case of tau decays we only have to consider vector and axial-vector contributions of decays into up, down and strange quarks. Thus taking i,j as the flavour indices for the light quarks (u, d and s) we can express the two-point function as

$$\Pi^{V/A}_{\mu\nu,ij}(s) \equiv i\int dx\, e^{ipx}\langle\Omega|T\{J^{V/A}_{\mu,ij}(x)J^{V/A}_{\nu,ij}(0)^\dagger\}|\Omega\rangle, \tag{3.1.5}$$

with $|\Omega\rangle$ being the physical vacuum. The vector and axial-vector currents are then distinguished by the corresponding dirac-matrices ($\gamma_\mu$and$\gamma_\mu\gamma_5$) given by

$$J^V_{\mu,ij}(x) = \bar{q}_j(x)\gamma_\mu q_i(x) \quad \text{and} \quad J^A_{\mu,ij}(x) = \bar{q}_j(x)\gamma_\mu\gamma_5 q_i(x). \tag{3.1.6}$$

With **??** we have a suitable physical quantity that can be theoretically as experimentally obtained. As the circle contour integral we used is has a radius of s_0 we successfully avoided low energies at which the application of pt would be questionable. For example if we would choose a radius with the size of the tau mass $m_\tau \approx 1.78\,MeV$ the strong coupling would have a perturbatively safe value of $\alpha_s(m_\tau) \approx 0.33$ [48]. Obviously we would benefit even more from a contour integral over a bigger circumference, but tau decays are limited by their mass. Nevertheless there are promising e^+e^- annihilation data, which yields valuable R-ratio values up to $2\,GeV$ [9][37].

3.1.2 Renormalisation Group Invariance

We have seen in section 2.2, that the two-point function is not a physical quantity. From the dispersion relation (eq. 2.4.2) we saw that it contains a unphysical polynom. Luckily for the vector correlator we are using in hadronic tau

decays the polynom is just a constant. Consequently by taking the derivative with respect to the momentum s we can derive a physical quantity from the two-point function:

$$D(s) \equiv -s\frac{d}{ds}\Pi(s). \tag{3.1.7}$$

$D(s)$ is called the *Adler function* and fulfils the RGE (eq. 2.1.11). The Adler function commonly has separte definitions for the longitudinal plus transversal and the solely longitudinal part contributions:

$$D^{(T+L)}(s) \equiv -s\frac{d}{ds}\Pi^{(T+L)}(s), \qquad D^{(L)}(s) \equiv \frac{s}{m_\tau^2}\frac{d}{ds}(s\Pi^{(L)}(s)). \tag{3.1.8}$$

The two-point functions in **??** can now be replaced with the help of partial integration

$$\int_a^b u(x)V(x)\,dx = \left[U(x)V(x)\right]_a^b - \int_a^b U(x)v(x)\,dx. \tag{3.1.9}$$

We will do the computation for each of the two cases $(T+L)$ and (L) separate. Starting by the transversal plus longitudinal contribution we get:

$$\begin{aligned} R_\tau^{(1)} &= \frac{6\pi i}{m_\tau^2}\oint_{|s|=m_\tau^2} \underbrace{\left(1-\frac{s}{m_\tau^2}\right)^2\left(1+2\frac{s}{m_\tau^2}\right)}_{=u(x)}\underbrace{\Pi^{(L+T)}(s)}_{=V(x)} \\ &= \frac{6\pi i}{m_\tau^2}\left\{\left[-\frac{m_\tau^2}{2}\left(1-\frac{s}{m_\tau^2}\right)^3\left(1+\frac{s}{m_\tau^2}\right)\Pi^{(L+T)}(s)\right]_{|s|=m_\tau^2}\right. \\ &\quad \left.+\oint_{|s|=m_\tau^2}\underbrace{-\frac{m_\tau^2}{2}\left(1-\frac{s}{m_\tau^2}\right)^3\left(1+\frac{s}{m_\tau^2}\right)}_{=U(x)}\underbrace{\frac{d}{ds}\Pi^{(L+T)}(s)}_{=v(x)}\right\} \\ &= -3\pi i\oint_{|s|=m_\tau^2 s}\frac{ds}{s}\left(1-\frac{s}{m_\tau^2}\right)^3\left(1+\frac{s}{m_\tau^2}\right)\frac{d}{ds}D^{(L+T)} \end{aligned} \tag{3.1.10}$$

where we fixed the integration constant to $C = -\frac{m_\tau^2}{2}$ in the second line and left the antiderivatives contained in the squared brackets untouched. If we parameterizing the integral appearing in the expression in the squared brackets we can see that it vanishes:

$$\left[-\frac{m_\tau^2}{2}\left(1-e^{-i\phi}\right)^3\left(1+e^{-i\phi}\right)\Pi^{(L+T)}(m_\tau^2 e^{-i\phi})\right]_0^{2\pi} = 0 \tag{3.1.11}$$

where $s \to m_\tau^2 e^{-i\phi}$ and $(1-e^{-i\cdot 0}) = (1-e^{-i\cdot 2\pi}) = 0$. Repeating the same calculation for the longitudinal part yields

$$\begin{aligned} R_\tau^{(L)} &= \oint_{|s|=m_\tau^2} ds \left(1-\frac{s}{m_\tau^2}\right)^2 \left(-\frac{2s}{m_\tau^2}\right) \Pi^{(L)}(s) \\ &= -4\pi i \oint \frac{ds}{s} \left(1-\frac{s}{m_\tau^2}\right)^3 D^{(L)}(s) \end{aligned} \tag{3.1.12}$$

Consequently combining the two parts results in

$$R_\tau = -\pi i \oint_{|s|=m_\tau^2} \frac{ds}{s} \left(1-\frac{s}{m_\tau^2}\right)^3 \left[3\left(1+\frac{s}{m_\tau^2} D^{(L+T)}(s) + 4D^{(L)}(s)\right)\right]. \tag{3.1.13}$$

It is convenient to define $x = s/m_\tau^2$ such that we can rewrite the inclusive ratio as

$$R_\tau = -\pi i \oint_{|s|=m_\tau^2} \frac{dx}{x}(1-x)^3 \left[3(1+x)D^{(L+T)}(m_\tau^2 x) + 4D^{(L)}(m_\tau^2 x)\right], \tag{3.1.14}$$

which will be the final expression we will be using to express the inclusive tau decay ratio.

3.2 Theoretical computation of R_τ

The previously derived expression for the tau decay ratio can be further organised in different δ contributions

$$R_{\tau,V/A}^{\omega} = \frac{N_c}{2} S_{EW} |V_{ud}|^2 \left(1 + \delta_\omega^{(0)} + \delta_\omega^{EW} + \delta_\omega^{DVs} + \sum_{D\leqslant 2} \delta_{ud,\omega}^{(D)}\right), \tag{3.2.1}$$

where $\delta^{(0)}$ is the perturbative contribution, $\delta^{(EW)}$ is a electroweak correction, $\delta^{(DV)}$ is the duality violation correction and $\delta^{(D)}$ are the higher dimensional contributions from the OPE. Note that in this work we will assume $\mathtt{delta}^{(DV)}$ to be negligible small for the weights we will apply.

We now want to derive the theoretical expressions needed to calculate every contribution to eq. 3.2.8 starting with the perturbative contribution.

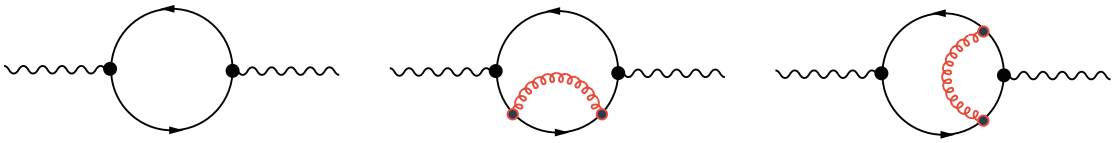

(a) (b) (c)

3.2.1 The perturbative contribution

We will treat the correlator in the chiral limit, in which the scalar and pseudo-scalar contribution of the two-point function vanish and the axial and vectorial contributions are equal. As a result we can focus ourselves of the vector correlation function two-point function $\Pi_V(s)$, which can be expanded as a sum over different orders of α [6]:

$$\Pi_V^{T+L}(s) = -\frac{N_c}{12\pi^2}\sum_{n=0}^{\infty} a_\mu^n \sum_{k=0}^{n+1} c_{n,k} L^k \quad \text{with} \quad L \equiv \ln\frac{-s}{\mu^2}. \tag{3.2.2}$$

The coefficient $c_{n,k}$ up to two-loop order can be obtained by Feynman diagram calculations. With the diagrams of **??** can calculate the zero-loop result of the correlator [34]

$$\Pi_{\mu\nu}^B(q^2)\Big|^{1-\text{loop}} = \frac{N_c}{12\pi^2}\left(\frac{1}{\hat{\epsilon}} - \log\frac{(-q^2 - i0)}{\mu^2} + \frac{5}{3} + \mathcal{O}(\epsilon)\right), \tag{3.2.3}$$

where $\Pi_{\mu\nu}^B(q^2)$ is the bare two-point function and is not renormalised[1] This result can then be used to extract the first two coefficients of the correlator expansion given in eq. 3.3.1

$$c_{00} = -\frac{5}{3} \qquad \text{and} \qquad c_{01} = 1. \tag{3.2.4}$$

The second loop can also be calculated by diagram techniques resulting in [7]

$$\Pi_V^{(1+0)}(s)\Big|^{2-\text{loop}} = -\frac{N_c}{12\pi^2} a_\mu \log(\frac{-s}{\mu^2}) + \cdots \tag{3.2.5}$$

yielding $c_{11} = 1$.

Beginning from three loop diagrams the algebra becomes exhausting and one has to use dedicated algorithms to compute the higher loops. The third loop calculations have been done in the late seventies by [17, 25, 16]. The four loop

[1] The term $1/\hat{\epsilon}$, which is of order zero in α_s, will be cancelled by renormalisation.

evaluation have been completed a little more than ten years later by [30, 58]. The highest loop published, that amounts to α_s^4, was published in 2008 [4] almost 20 years later.

Fixing the number of colors to $N_c = 3$ the missing coefficients up to order four in α_s read:

$$\begin{aligned} c_{2,1} &= \frac{365}{24} - 11\zeta_3 - \left(\frac{11}{12} - \frac{2}{3}\zeta_3\right) N_f \\ c_{3,1} &= \frac{87029}{288} - \frac{1103}{4}\zeta_3 + \frac{275}{6}\zeta_5 \\ &\quad - \left(\frac{7847}{216} - \frac{262}{9}\zeta_3 + \frac{25}{9}\zeta_5\right) N_f + \left(\frac{151}{162} - \frac{19}{27}\zeta_3\right) N_f^2 \\ c_{4,1} &= \frac{78631453}{20736} - \frac{1704247}{432}\zeta_3 + \frac{4185}{8}\zeta_3^2 + \frac{34165}{96}\zeta_5 - \frac{1995}{16}\zeta_7, \end{aligned} \tag{3.2.6}$$

where used the flavor number $N_f = 3$ for the last line.

The 6-loop calculation has until today not been achieved, but Beneke and Jamin [6] used and educated guess to estimate the coefficient

$$c_{5,1} \approx 283 \pm 283. \tag{3.2.7}$$

In stating the coefficients $c_{n,k}$ of the correlator expansion we have restricted ourselves to k-indices equal to one. This is due to the RGE, which relates coefficients with k different than one to the already stated coefficients $c_{n,1}$. To relate the coefficients we have to make use of the RGE. Consequently the correlator $\Pi_V^{T+L}(s)$ needs to be a physical quantity, which we can be achieved with the previously defined Adler function (eq. 3.2.1). The correct expression for the correlator expansion in eq. 3.3.1 is then given by

$$D_V^{(T+L)} = -s\frac{d\Pi_V^{(T+L)}(s)}{ds} = \frac{N_c}{12\pi^2}\sum_{n=0}^{\infty} a_\mu^n \sum_{k=1}^{n+1} k c_{n,k} L^{k-1}, \tag{3.2.8}$$

where we used $dL^k/ds = k\ln(-s/\mu^2)^{k-1}(-1/\mu^2)$. Applying the RGE (**??**) to the scale-invariant Adler function yields

$$-\mu\frac{d}{d\mu}D_V^{(T+L)} = -\mu\frac{d}{d\mu}\left(\tfrac{\partial}{\partial L}\,dL + \tfrac{\partial}{\partial a_s}\,da_s\right) D_V^{T+L} = \left(2\tfrac{\partial}{\partial L} + \beta\tfrac{\partial}{\partial a_s}\right) D_V^{T+L} = 0, \tag{3.2.9}$$

where we made use of the β function, which is defined in eq. 2.1.12, and of the expression $dL/d\mu = -2/\mu$.

The relation between the correlator expansion coefficients can then be taken by calculating the Adler function for a desired order and plugging it into the RGE. For example the Adler function to the second order in α_s

$$D(s) = \frac{N_c}{12\pi^2}\left[c_{01} + a_\mu(c_{11} + 2c_{12}L) + a_\mu^2(c_{21} + 2c_{22}L + 3c_{23}L^2)\right], \tag{3.2.10}$$

can be inserted into RGEAdler

$$4a_\mu c_{12} + 2a_\mu^2(2c_{22} + 6c_{23}L) + \beta_1 a_\mu^2(c_{11} + 2c_{12}L) + \mathcal{O}(a_\mu^3) = 0 \tag{3.2.11}$$

to compare the coefficients order by order in α_s. At order α_μ only the c_{12} term is present and has consequently to be zero. For $\mathcal{O}(a_\mu^2 L)$ only c_{23} exists as $c_{12} = 0$ and thus also has to vanish. Finally at $\mathcal{O}(a)$ we can relate c_{22} with c_{11} resulting in:

$$c_{12} = 0, \quad c_{22} = \frac{\beta_1 c_{11}}{4} \quad \text{and} \quad c_{23} = 0. \tag{3.2.12}$$

Implementing the newly obtained Adler coefficients we can write out the Adler function to the first order:

$$D(s) = \frac{N_c}{12\pi^2}\left[c_{01} + c_{11}a_\mu\left(c_{21} - \frac{1}{2}\beta_1 c_{11}L\right)a_\mu^2\right] + \mathcal{O}(a_\mu^3). \tag{3.2.13}$$

continue here We have used the RGE to relate Adler-function coefficients and thus reduce its numbers. But as we will see in the following section the RGE gives us two different choices in the order of the computation of the perturbative contribution to the inclusive tau decay ratio.

Renormalization group summation

By making use of the RGE we have to decide about the order of mathematical operations we perform. As the perturbative contribution $\delta^{(0)}$ is independent on the scale μ we are confronted with two choices *fixed-order perturbation theory* (FOPT) or *contour-improved perturbation theory* (CIPT). Each of them yields a different result, which is the main source of error in extracting the strong coupling from tau decays.

We can write the perturbative contribution $\delta^{(0)}$ of R_τ (eq. 3.2.8) in the chiral limit, such that the longitudinal contribution $D^{(L)}$, in eq. 3.2.7 vanishes. Thus

inserting the expansion of $D_V^{(T+L)}$ into the hadronic tau decay width eq. 3.2.7 yields

$$\delta^{(0)} = \sum_{n=1}^{\infty} a_\mu^n \sum_{k=1}^{n} k c_{n,k} \frac{1}{2\pi i} \oint_{|x|=1} \frac{dx}{x} (1-x)^3 (1+x) \log\left(\frac{-m_\tau^2 x}{\mu^2}\right)^{k-1}. \tag{3.2.14}$$

Keep in mind that the contributions from the vector and axial-vector correlator are identical in the massless case:

$$D^{(T+L)} = D_V^{(T+L)} + D_A^{(T+L)} = 2D_V^{(T+L)}. \tag{3.2.15}$$

To continue evaluating the perturbative part we can now either follow the description of FOPT or CIPT. We will now present both.

In FOPT we fix the scale at the tau mass ($\mu^2 = m_\tau^2$), which leaves us with the integration over the logarithm, as seen in

$$\delta_{FO}^{(0)} = \sum_{n=1}^{\infty} a(m_\tau^2)^n \sum_{k=1}^{n} k c_{n,k} J_{k-1} \tag{3.2.16}$$

where the contour integrals J_l are defined by

$$J_l \equiv \frac{1}{2\pi i} \oint_{|x|=1} \frac{dx}{x} (1-x)^3 (1+x) \log^l(-x). \tag{3.2.17}$$

The integrals J_l up to order α_s^4 are given by [6]:

$$J_0 = 1, \quad J_1 = -\frac{19}{12} \quad J_2 = \frac{265}{72} - \frac{1}{3}\pi^2, \quad J_3 = -\frac{3355}{288} + \frac{19}{12}\pi^2. \tag{3.2.18}$$

Using FOPT the strong coupling $a(\mu)$ is fixed at the tau mass scale $a(m_\tau^2)$ and can be taken out of the closed-contour integral. Thus we solely have to integrate over the logarithms $\log(x)$.

Using CIPT we can sum the logarithms by setting the scale to $\mu^2 = -m_\tau^2 x$ in eq. 3.3.13, resulting in:

$$\delta_{CI}^{(0)} = \sum_{n=1}^{\infty} c_{n,1} J_n^a(m_\tau^2), \tag{3.2.19}$$

where the contour integrals J_l are defined by

$$J_n^a(m_\tau^2) \equiv \frac{1}{2\pi i} \oint_{|x|=1} \frac{dx}{x} (1-x)^3 (1+x) a^n(-m_\tau^2 x). \tag{3.2.20}$$

Note that all logarithms vanish, except the ones with index $k = 1$:

$$\log(1)^{k-1} = \begin{cases} 1 & \text{if } k = 1, \\ 0 & k \neq 1 \end{cases} \tag{3.2.21}$$

which selects the Adler function coefficients $c_{n,1}$. Handling the logarithms left us with the integration of $\alpha_s(-m_\tau^2 x)$ over the closed-contour $\oint_{|x|=1}$, which now depends on the integration variable x.

In general we have to decide if we want to perform a contour integration with a constant coupling constant and variable logarithms (FOPT) or "constant logarithms" and a running coupling (CIPT). To emphasize the differences in both approaches we can calculate the perturbative contribution $\delta^{(0)}$ to R_τ for the two different prescriptions yielding [6]

$$\begin{array}{cccccc} & \alpha_s^2 & \alpha_s^2 & \alpha_s^3 & \alpha_s^4 & \alpha_s^5 \\ \delta_{FO}^{(0)} = & 0.1082 & + 0.0609 & + 0.0334 & + 0.0174 (+0.0088) & = 0.2200 (0.2288) \end{array} \tag{3.2.22}$$

$$\delta_{CI}^{(0)} = 0.1479 + 0.0297 + 0.0122 + 0.0086 (+0.0038) = 0.1984 (0.2021). \tag{3.2.23}$$

The series indicate, that CIPT converges faster and that both series approach a different value. This discrepancy represents currently the biggest theoretical uncertainty while extracting the strong coupling.

As today we do not know if FOPT or CIPT is the correct approach of measuring the strong coupling. Therefore there are currently three ways of stating results: Quoting the average of both results, quoting the CIPT result or quoting the FOPT result. We follow the approach of Beneke and Jamin [6] who prefere FOPT, but also state their results in CIPT.

3.2.2 The Non-Perturbative OPE Contribution

The perturbative contribution to the Sum-Rule, that we have seen so far, is the dominant one. With

$$\begin{aligned} R_\tau^{FOPT} &= \\ R_\tau^{CIPT} &= \end{aligned} \tag{3.2.24}$$

The NP vs perturbative contributions can be varied by chosen different weights than ω_τ.

3.2.3 Dimension four

For the OPE contributions of dimension four we have to take into account the terms with masses to the fourth power m^4, the quark condensate multiplied

by a mass $m\langle\overline{q}\,q\rangle$ and the gluon condensate $\langle GG\rangle$. The resulting expression can be taken from the appendix of [47], yielding:

$$D_{ij}^{(L+T)}(s)\Big|_{D=4} = \frac{1}{s^2}\sum_n \Omega^{(1+0)}(s/\mu^2)a^n, \tag{3.2.25}$$

where

$$\begin{aligned}\Omega_n^{(1+0)}(s/\mu^2) \;=\; & \frac{1}{6}\langle aGG\rangle p_n^{(L+T)}(s/\mu^2) + \sum_k m_k\langle\overline{q}_k q_k\rangle r_n^{(L+T)}(s/\mu^2)\\ & + 2\langle m_i\overline{q}_i q_i + m_j\overline{q}_j q_j\rangle q_n^{(L+T)}(s/\mu^2) \pm \frac{8}{3}\langle m_j\overline{q}_i q_i + m_i\overline{q}_j q_j\rangle t_n^{(L+T)}\\ & - \frac{3}{\pi^2}(m_i^4 + m_j^4)h_n^{(L+T)}(s/\mu^2) \mp \frac{5}{\pi^2}m_i m_j(m_i^2+m_j^2)k_n^{(L+T)}(s/\mu^2)\\ & + \frac{3}{\pi^2}m_i^2 m_j^2 g_n^{(L+T)}(s/\mu^2) + \sum_k m_k^4 j_n^{(L+T)}(s/\mu^2) + 2\sum_{k\neq l} m_k^2 m_l^2 u_n^{(L+T)}(s/\mu^2)\end{aligned} \tag{3.2.26}$$

The perturbative expansion coefficients are known to $\mathcal{O}(a^2)$ for the condensate contributions,

$$\begin{array}{lll} p_0^{(L+T)} = 0, & p_1^{(L+T)} = 1, & p_2^{(L+T)} = \frac{7}{6},\\ r_0^{(L+T)} = 0, & r_1^{(L+T)} = 0, & r_2^{(L+T)} = -\frac{5}{3} + \frac{8}{3}\zeta_3 - \frac{2}{3}\log(s/\mu^2),\\ q_0^{(L+T)} = 1, & q_1^{(L+T)} = -1, & q_2^{(L+T)} = -\frac{131}{24} + \frac{9}{4}\log(s/\mu^2)\\ t_0^{(L+T)} = 0 & t_1^{(L+T)} = 1, & t_2^{(L+T)} = \frac{17}{2} + \frac{9}{2}\log(s/\mu^2).\end{array} \tag{3.2.27}$$

while the m^4 terms have been only computed to $\mathcal{O}(a)$

$$\begin{array}{ll} h_0^{(L+T)} = 1 - 1/2\log(s/\mu^2), & h_1^{(L+T)} = \frac{25}{4} - 2\zeta_3 - \frac{25}{6}\log(s/\mu^2) - 2\log(s/\mu^2)^2,\\ k_0^{(L+T)} = 0, & k_1^{(L+T)} = 1 - \frac{2}{5}\log(s/\mu^2),\\ g_0^{(L+T)} = 1, & g_1^{(L+T)} = \frac{94}{9} - \frac{4}{3}\zeta_3 - 4\log(s/\mu^2),\\ j_0^{(L+T)} = 0, & j_1^{(L+T)} = 0,\\ u_0^{(L+T)} = 0, & u_2^{(L+T)} = 0.\end{array} \tag{3.2.28}$$

3.2.4 Dimension six and eight

Our application of dimension six contributions is founded in [12] and has previously been calculated beyond leading order by [38]. The operators appearing are the masses to the power six m^6, the four-quark condensates $\langle\overline{q}\,q\overline{q}\,q\rangle$, the three-gluon condensates $\langle g^3G^3\rangle$ and lower dimensional condensates multiplies

by the corresponding masses, such that in total the mass dimension of the operator will be six. As there are too many parameters to be fitted with experimental data we have to omit some of them, starting with the three-gluon condensate, which does not contribute at leading order. The four-quark condensates known up to $\mathcal{O}(\alpha^2)$, but we will make use of the *vacuum saturation approach* [6, 12, 56] to express them in quark, anti-quark condensates $\langle q\overline{q}\rangle$. In our work we take the simplest approach possible: Introducing an effective dimension six coefficient $\rho^{(6)}_{V/A}$ divided by the appropriate power in s

$$D^{(1+0)}_{ij,V/A}\Big|_{D=6} = 0.03\frac{\rho^{(6)}_{V/A}}{s^3} \tag{3.2.29}$$

As for the dimension eight contribution the situation is not better than the dimension six one we keep the simplest approach, leading to

$$D^{(1+0)}_{ij,V/A}\Big|_{D=8} = 0.04\frac{\rho^{(8)}_{V/A}}{s^4}. \tag{3.2.30}$$

3.2.5 Duality Violations

3.3 Experiment

The τ-decay data we use to perform our QCD-analysis is from the **ALEPH** experiment. The ALEPH experiment was located at the large-electron-positron (LEP) collider at CERN laboratory in Geneva. LEP started producing particles in 1989 and was replaced in the late 90s by the large-hadron-collider, which makes use of the same tunnel of 27km circumference. The data produced within the experiment is still maintained by former ALEPH group members under led by M. Davier, which have performed regular updates on the data-sets [23, 20, 51].

The measured spectral functions for the Aleph data are defined in [21] and

given for the transverse and longitudinal components separately:

$$\begin{aligned}\rho_{V/A}^{(T)}(s) = &\frac{m_\tau^2}{12\left|V_{ud}^2\right| S_{EW}} \frac{\mathcal{B}(\tau^- \to V^-/A^- \nu_\tau)}{\mathcal{B}(\tau^- \to e^- \overline{\nu}_e \nu_\tau)} \\ &\times \frac{dN_{V/A}}{N_{V/A}\, ds} \left[\left(1 - \frac{s}{m_\tau^2}\right)^2 \left(1 + \frac{2s}{m_\tau^2}\right)\right]^{-1} \\ \rho_A^{(L)}(s) = &\frac{m_\tau^2}{12\left|V_{ud}^2 S_{EW}\right|} \frac{\mathcal{B}(\tau^- \to \pi^-(K^-)\nu_\tau)}{\mathcal{B}(\tau^- \to e^- \overline{\nu}_e \nu_\tau)} \times \frac{dN_A}{N_A\, ds} \left(1 - \frac{s}{m_\tau^2}\right)^{-2}.\end{aligned} \tag{3.3.1}$$

$$\mathcal{B}_e = ... \tag{3.3.2}$$

$$R_{\tau,V/A} = \frac{B_{V/A,\tau}}{B_e} \tag{3.3.3}$$

The data relies on a separation into vector and axial-vector channels. In the case of the Pions this can be achieved via counting. The vector channel is characterised by a negative parity, whereas the axial-vector channel has positive parity. A quark has by definition positive parity, thus an anti-quark has a negative parity. A meson, like the Pion particle, is a composite particle consisting of an quark an anti-quark. Consequently a single Pion carries negative parity, an even number of Pions carries positive parity and an odd number of Pions carries negative parity:

$$n \times \pi = \begin{cases} \text{vector} & \text{if } n \text{ is even,} \\ \text{axial-vector} & \text{otherwise} \end{cases}. \tag{3.3.4}$$

The contributions to the vector and axial channel can be seen in figure. The dominant modes in the vector case are [22] $\tau^- \to \pi^-\pi^0\nu_\tau$ and the $\tau^- \to \pi^-\pi^-\pi^+\pi^0\nu_\tau$. The first of these is produced by the $\rho(770)$ meson, which in contrary to the pions carries angular momentum of one, which is also clearly visible as peak around 770 GeV in figure vector. The dominant modes in the axial-vector case are $\tau^- \to \pi^-\nu_\tau$, $\tau^- \to \pi^-\pi^0\pi^0\nu_\tau$ and $\tau^- \to \pi^-\pi^-\pi^+\nu_\tau$. Here the three pion final states stem from the a_1^--meson, which is also clearly visible as a peak in figure.

wavy => DV OPE cannot reproduce suppressed in VpA regions below 1.5 GeV can still not be applied

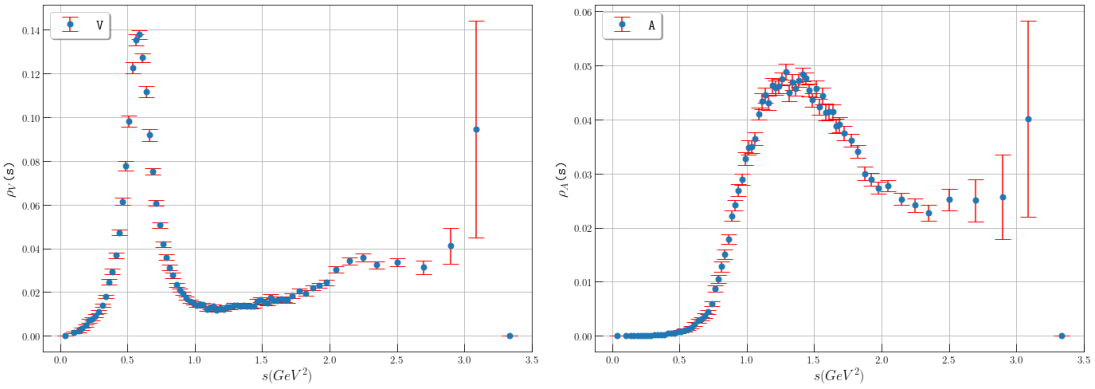

(a) A gull (b) A mouse

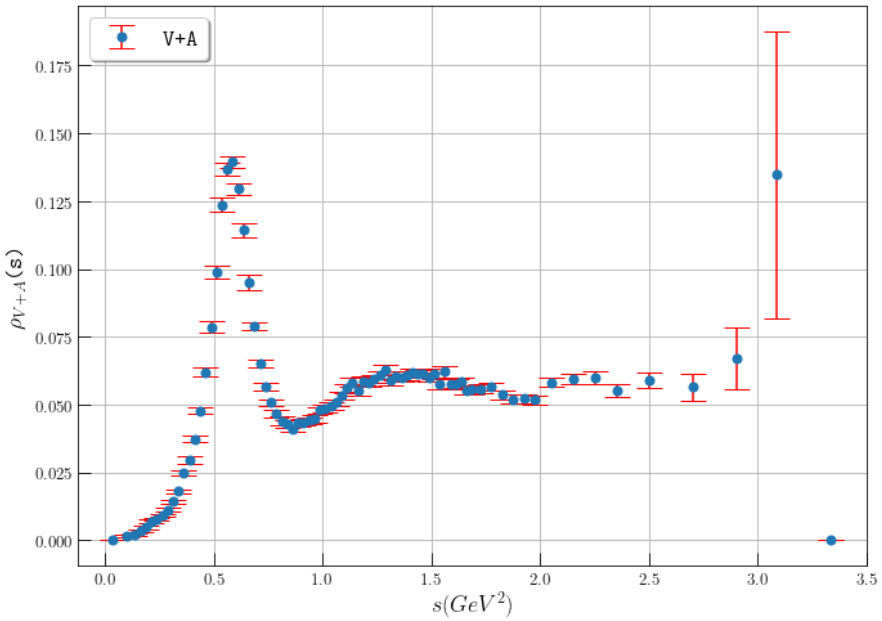

Figure 3.1: Pictures of animals

The different inclusive τ-decay ratios are then given by

$$R_{\tau,V} = ... \tag{3.3.5}$$

Chapter 4

Measuring the strong coupling

4.1 Fits

In the following we will perform fits to determine α_s at the m_τ^2-scale. The fits are separated corresponding to the used weight. Every weight contains multiple fits for different s_0-momenta. We will start with the kinematic weight, which appears naturally in the inclusive τ-decay ratio eq. 3.1.1 and has the best fitting characteristics of all weights we have used.

4.1.1 Kinematic weight: $\omega_\tau(x) \equiv (1-x)^2(1+2x)$

The kinematic weight is defined as $\omega(x) = (1-x)^2(1+2x)$. It is a double pinched, polynomial weight-function that contains the unity and does not contain a term proportional to x, which makes it an optimal weight [5]. As a doubled pinched weight it should have a good suppression of DV-contributions and its polynomial contains terms proportional to x^2 and x^3, which makes it sensitive to the dimension six and eight OPE contributions. The fits have been performed within the framework of FOPT for different numbers of s_0. The momentum sets are characterised by its lowest energy s_{min}. We fitted values down to 1.5 GeV. Going to lower energies is questionable due to the coupling constant becoming to large, which implies a breakdown of PT and appearing DVs. Furthermore it bares the risk to be affected by the $\rho(770)$ and a_1 peaks in the vector and axial-vector spectral function, which we cannot model within the framework of the OPE. For the fitting-parameters α_s, c_6 and

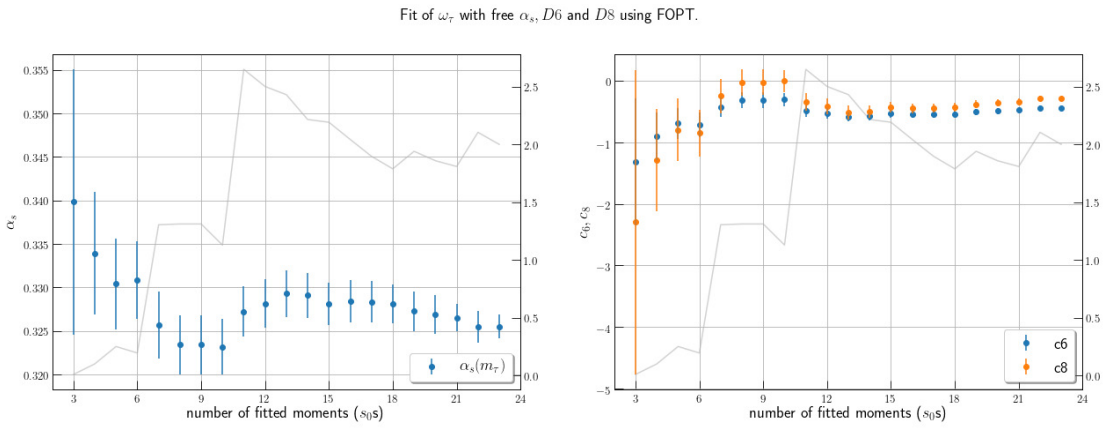

Figure 4.1: Fitting values of $\alpha_s(m_\tau^2), c_6$ and c_8 for the kinematic weight $\omega(x) = (1-x)^2(1+2x)$ using FOPT for different s_{min}. The left graph plots $\alpha_s(m_\tau^2)$ for different numbers of used s_0s. The right plot contains the dimension six and eight contributions to the OPE. Both plots have in grey the χ^2 per degree of freedom (dof).

c_8 we have given the results in table 4.1 and graphically in fig. 4.1.

s_{min}	#s_0s	$\alpha_s(m_\tau^2)$	c_6	c_8	χ^2/dof
1.950	10	0.3232(32)	-0.31(11)	-0.01(18)	1.13
2.000	9	0.3234(34)	-0.32(12)	-0.03(21)	1.31
2.100	8	0.3256(38)	-0.43(15)	-0.25(28)	1.30
2.200	7	0.3308(44)	-0.72(20)	-0.85(38)	0.19
2.300	6	0.3304(52)	-0.69(25)	-0.80(50)	0.25
2.400	5	0.3339(70)	-0.91(39)	-1.29(83)	0.10
2.600	4	0.3398(15)	-1.3(1.0)	-2.3(2.5)	0.01

Table 4.1: Table of our fitting values of $\alpha_s(m_\tau^2), c_6$ and c_8 for the kinematic weight $\omega(x) = (1-x)^2(1+2x)$ using FOPT ordered by increasing s_{min}. The errors are given in parenthesis after the observed value.

We only display the fits for s_{min} larger than 1.95 GeV as fits with higher s_{min} have a too large χ^2 (larger than two). We achieved six good fits with a χ^2 per dof less or close to one, which we divided into two groups:

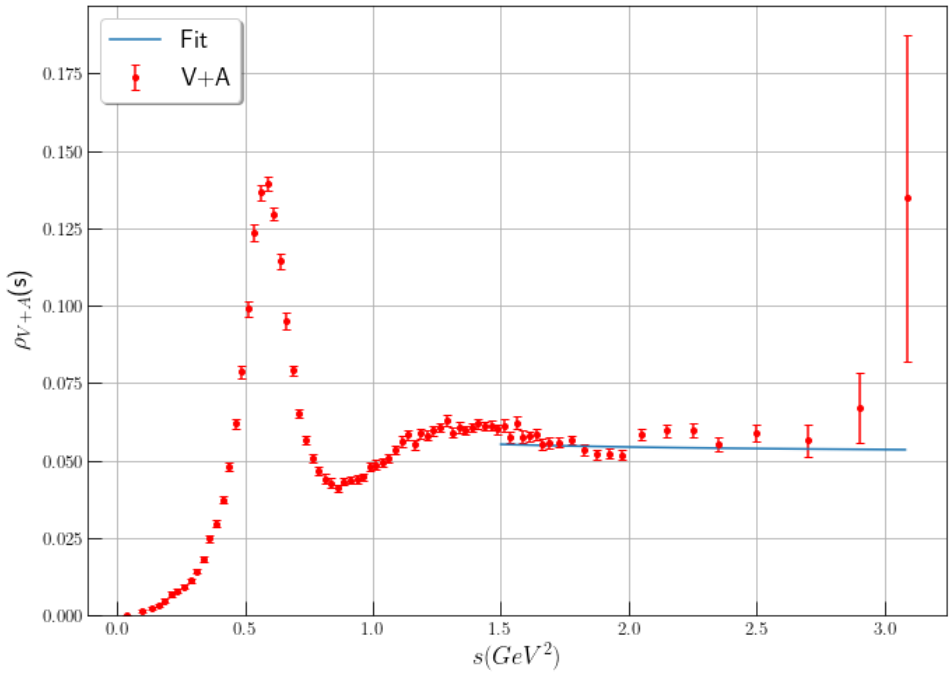

Figure 4.2: test

- Fits with **5-7** momenta have χ^2 per DOF larger than one and means of $\alpha(m_\tau^2) = 0.3317(33), c_6 = -0.77(17)$ and $c_8 = -0.98(35)$, where we propagated the uncertainty. We have excluded the momentum containing four s_0s, because it χ^2 is too low and its errors are too large, which is because we have to fix three variables for only four data points.

- Fits with **8-10** momenta have small χ^2 per DOF values and lower means for the strong coupling $\alpha(m_\tau^2) = 0.3241(20)$ but the OPE contributions are higher $c_6 = -0.350(75)$ and $c_8 = -0.09(12)$.

The values for the less momenta are preferred by us due to two reasons. First below energies of 2.2 GeV we have to face the problematic influence of increasing resonances. Second, we will see, that the values obtained from the lower moment fits are more compatible with our other fits series. For both, the momenta sets, we see a good convergence of the OPE.

We further tested the stability of the dimension six and eight contributions to the OPE within the same fit series but for a fixed value of the strong coupling

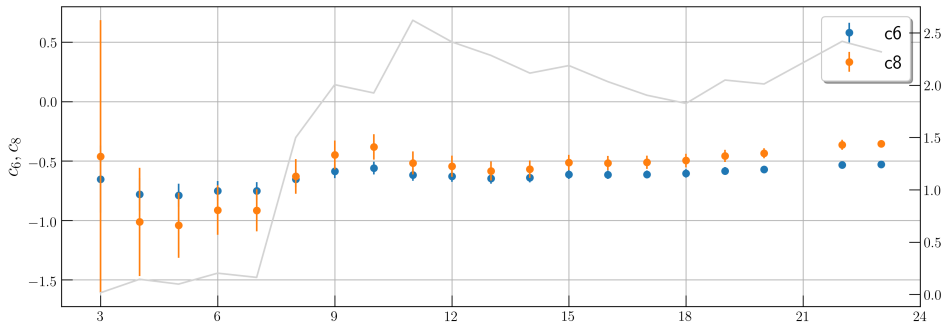

Figure 4.3

to our previous averaged result $\alpha_s(m_\tau^2) = 0.3179$. The fits have been plotted in fig. 4.3 and show good stability. The values for c_6 and c_8 are larger than the values given in our final results from table 4.1. This is explained with a smaller contribution from the strong coupling (α_s is smaller), which has to be compensated by larger OPE contributions.

Due to the good results we will try to argue in favour of the values obtained by the lower momenta:

$$\alpha_s(m_\tau^2) = 0.3317(33), \quad c_6 = -0.77(17) \quad \text{and} \quad c_8 = -0.98(35). \tag{4.1.1}$$

4.1.2 Cubic weight: $\omega_{\text{cube}}(x) \equiv (1-x)^3(1+3x)$

To further consolidate the results from the kinematic weight, we test a weight of higher pinching, which is known to suppress DV more than a double pinched weight would do. Consequently, any differences to the previous fit could indicate a problem with the DV treatment. Our *cubic* weight will be triple pinched and optimal, as the kinematic weight is double pinched and we do not want any problematic contributions proportional to x. Thus we define the *cubic weight* as $\omega_{\text{cube}}(x) \equiv (1-x)^3(1+3x)$. It is due to its polynomial structure sensitive to the dimensions six, eight and ten contributions of the OPE, which yields one more parameter to fit than with the kinematic weight ω_τ. The some good, selected fits, by χ^2 per DOF, can be seen in table 4.2 and graphically in section 4.1.2. As with the kinematic weight we get two different sets of value:

- The fits with **9, 10 and 11** momenta have a too high χ^2, but are compa-

s_{min}	$\#s_0s$	$\alpha_s(m_\tau^2)$	c_6	c_8	c_{10}	χ^2/dof
1.900	11	0.3249(29)	-0.280(20)	-0.088(21)	0.088(55)	1.58
1.950	10	0.3237(26)	-0.232(25)	0.005(42)	0.275(93)	1.67
2.000	9	0.3228(26)	-0.196(27)	0.075(28)	0.420(56)	1.96
2.100	8	0.3302(40)	-0.52(11)	-0.58(22)	-1.00(45)	0.43
2.200	7	0.3312(43)	-0.56(12)	-0.68(23)	-1.23(50)	0.55
2.300	6	0.336(11)	-0.78(47)	-1.17(98)	-2.38(22)	0.29
2.400	5	0.3330(96)	-0.63(47)	-0.82(10)	-1.51(26)	0.48

Table 4.2: Table of our fitting values of $\alpha_s(m_\tau^2), c_6$, c_8 and c_{10} for the cubic weight $\omega(x) = (1-x)^3(1+3x)$ using FOPT ordered by increasing s_{min}. The errors are given in parenthesis after the observed value.

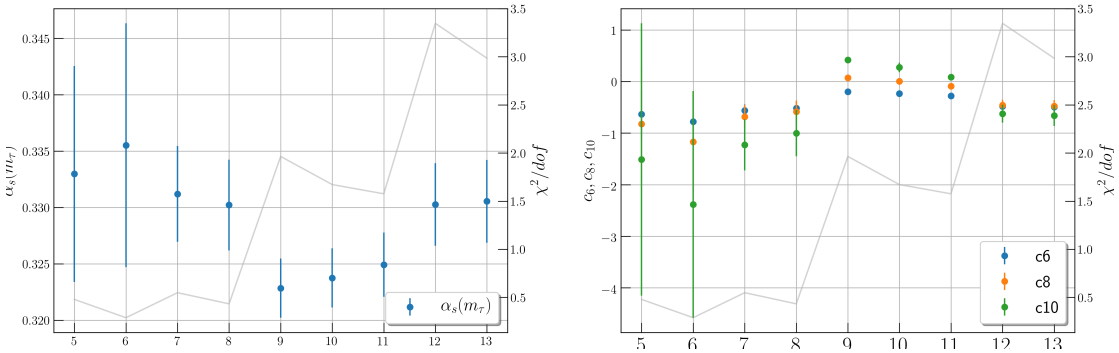

rable to our the upper entries of the kinematic weight table table 4.1. As with the kinematic weight the s_{min} seems to be affected by lower resonances.

- The fits with **5,6,7 and 8** have a better χ^2 per DOF value and are in good agreement with the corresponding fits of the kinematic weight. The averaged value with its propagated errors read: $\alpha_s(m_\tau^2) = 0.332478(61), c_6 = -0.622(12), c_8 = -0.815(55)$ and $c_{10} = -1.5(3.1)$.

We furthermore found that the OPE is converging, but not as good as for the kinematic weight. The values of $\left|\delta^{(8)}\right|$ is only half as large as $\left|\delta^{(8)}\right|$. The values of the lower momentum count are in high agreement with the ones obtained from the kinematic weight. The conclusions that we take from the *cubic weight* are that the kinematic weight, with its double pinching, should sufficiently suppress any contributions from DVs. If DV would have an effect on the kinematic weight, we should have seen an improvement of the fits with the *cubic* weight, due to its triple pinching, which is not the case.

4.1.3 Quartic weight: $\omega(x) \equiv (1-x)^4(1+4x)$

To include an even higher pinching of four and to compare the previously obtained value for the dimension ten OPE contribution we performed fits with the *quartic weight* defined as $\omega(x) \equiv (1-x)^4(1+4x)$, which also fulfils the definition of an optimal weight [5]. Unfortunately the fits only converged for $s_{min} = 2\,GeV$ (nine s_0s moment combination). The results for , with a χ^2 per DOF of 0.67 are given by:

$$\begin{aligned} \alpha_s(m_\tau^2) = 0.3290(11), \quad c_6 = -0.3030(46), \quad c_8 = -0.1874(28), \\ c_{10} = 0.3678(45) \quad \text{and} \quad c_{12} = -0.4071(77) \end{aligned} \tag{4.1.2}$$

Due to the problematic of the fitting routing, which is caused by too many OPE contributions fitted simultaneously, we will discard the fitting results for the quartic weight.

s_{min}	#s0s	$\alpha_s(m_\tau^2)$	c_8	χ^2/dof
2.200	7	0.3214(49)	-1.01(39)	0.41
2.300	6	0.3227(57)	-1.18(54)	0.46
2.400	5	0.3257(67)	-1.58(74)	0.39
2.600	4	0.325(10)	-1.54(1.53)	0.58
2.800	3	0.326(21)	-1.69(4.03)	1.17

Table 4.3: Table of our fitting values of $\alpha_s(m_\tau^2)$, and c_8 for the single pinched third power monomial weight $\omega(x) = 1 - x^3$ using FOPT ordered by increasing s_{min}. The errors are given in parenthesis after the observed value.

4.1.4 Third power monomial: $\omega_{m3}(x) \equiv 1 - x^3$

To study the behaviour of the DV and the higher order OPE contributions of dimension eight and ten we further included two optimal, single pinched weights. The first one is defined as $\omega_{m3}(x) \equiv 1 - x^3$ and contains a single third power monomial and is consequently sensitive to dimension eight contributions from the OPE. Our fitting results can be taken from table 4.3. The χ^2 per DOF is like in the ω_τ and ω_{cubic} fits good for $s_{min} \leqslant 2.2\,GeV$, but jumps to values $\chi^2/dof > 1.4$ for smaller s_{min}. This is, as before, explained through resonances that appear in lower energies. Due to the good χ^2 and the internally compatible fitting values we averaged over all rows except the last one of table 4.3. The last row, at $s_{min} = 2.8\,GeV$ has only one DOF and thus high errors. The averaged values are thus given by

$$\alpha(m_\tau^2) = 0.32382(42) \qquad \text{and} \qquad c_8 = -1.33(67). \tag{4.1.3}$$

We note that the strong coupling is smaller as our expected values from the kinematic weight **??**, but the dimension eight contribution is in good agreement. The strong coupling from the monomial weight to third order seems to be in better agreement with the 8-10 momenta used in the kinematic fits, whereas the dimension eight contributions agrees more with the 4-7 momenta fits.

We have made use of a single pinched weight and discovered that the fitting

s_{min}	$\#s_0s$	$\alpha_s(m_\tau^2)$	c_{10}	χ^2/dof
2.200	7	0.3203(48)	-1.64(77)	0.42
2.300	6	0.3216(56)	-2.01(1.13)	0.47
2.400	5	0.3247(66)	-2.98(1.62)	0.39
2.600	4	0.324(10)	-2.86(3.69)	0.58
2.800	3	0.325(20)	-3.43(10.74)	1.17

Table 4.4: Table of our fitting values of $\alpha_s(m_\tau^2)$ and c_{10} for the single pinched fourth power monomial weight $\omega(x) = 1 - x^4$ using FOPT ordered by increasing s_{min}. The errors are given in parenthesis after the observed value.

result is not completely compatible with our previous fitting results. Consequently weights with a pinching less than two are affected by DV and should not be used to determine the strong coupling.

4.1.5 Fourth power monomial: $\omega_{m4}(x) \equiv 1 - x^4$

We already analysed the cubic and quartic weights, which depend on the dimension ten OPE contribution, in section 4.1.2 and section 4.1.3 correspondingly. Now, even with the visible DV for fourth power monomial $\omega_{m4} \equiv 1 - x^4$ to study another single pinched moment and the dimension ten OPE contribution. The results of the are given in **??**. The fitting behaviour is very similar to the third power monomial (**??**) and we will directly cite our obtained results:

$$\alpha_s(m_\tau^2) = 0.32277(40) \qquad \text{and} \qquad c_{10} = -2.4(3.6). \tag{4.1.4}$$

As before the values for the strong coupling are lower than the ones obtained by the kinematic weight fit. Furthermore the error on the tenth dimension contribution of the OPE are too huge, although the huge errors makes it compatible with all previous results. All in all the usage of the single pinched fourth power monomial weight is questionable and does not deliver any additional insights.

4.1.6 Pich's Optimal Moments [48]

Next to the previously mentioned *optimal weights* from Beneke and Jamin [5] there are *optimal moments* introduced by Pich [39]. Combinations of these optimal moments have been widely used by the ALEPH collaboration to perform QCD analysis on the Large electron-positron collider (LEP). These moments include the for FOPT problematic proportional term in x [5], thus we will perform additional fits in the Borel-sum.

$$\omega_{(n,m)}(x) = (1-x)^n \sum_{k=0}^{m} (k+1)x^k \tag{4.1.5}$$

$$\omega(x) = (1-x)^2$$

s_{min}	#s_0s	$\alpha_s(m_\tau^2)$	aGGInv	c_6	χ^2/dof
2.200	7	0.3401(57)	-0.0185(52)	0.220(88)	0.73
2.300	6	0.3383(68)	-0.0165(67)	0.26(12)	0.89
2.400	5	0.3450(93)	-0.0243(99)	0.10(17)	0.71
2.600	4	0.337(16)	-0.014(18)	0.36(45)	0.98

Table 4.5: Table of our fitting values of $\alpha_s(m_\tau^2)$, aGGInv and c_6 for the triple pinched optimal weight $\omega^{(2,0)}(x) = (1-x)^2$ using FOPT ordered by increasing s_{min}. The errors are given in parenthesis after the observed value.

$$\omega(x) = (1-x)^3$$

s_{min}	$\#s_0s$	$\alpha_s(m_\tau^2)$	$aGGI n\nu$	c_6	c_8	χ^2/dof
1.900	11	0.34281(92)	-0.01473(73)	-0.103(22)	-0.534(46)	1.52
1.950	10	0.34154(99)	-0.01304(61)	-0.050(17)	-0.389(44)	1.42
2.000	9	0.33985(81)	-0.01124(43)	0.002(10)	-0.242(26)	1.59
2.100	8	0.3480(47)	-0.0201(36)	-0.264(89)	-1.03(28)	0.31
2.200	7	0.3483(23)	-0.0204(41)	-0.27(15)	-1.05(40)	0.41
2.300	6	0.3522(64)	-0.0249(62)	-0.42(18)	-1.51(57)	0.29
2.400	5	0.3480(89)	-0.0199(100)	-0.25(33)	-0.96(10)	0.39

Table 4.6: Table of our fitting values of $\alpha_s(m_\tau^2), aGGI n\nu, c_6$ and c_8 for the optimal weight $\omega^{(3,0)}(x) = (1-x)^3$ using FOPT ordered by increasing s_{min}. The errors are given in parenthesis after the observed value.

weight	s_{min}	$\alpha_s(m_\tau^2)$	$a\langle GG\rangle_{inv}$	c_6	c_8	c_{10}	χ^2/dof
ω_{kin}	2.2	0.3308(44)	-	-0.72(20)	-0.85(38)	-	0.19
ω_{cube}	2.1	0.3302(40)	-	-0.52(11)	-0.58(22)	-1.00(45)	0.43
$\omega^*_{3,0}$	2.1	0.3239(30)	-0.2125(26)	-0.627(87)	-0.74(17)	-	0.46
$\omega_{quartic}$	2.0	0.3290(11)	-	-0.3030(46)	-0.1874(28)	0.3678(45)	0.67
ω_{m3}	2.2	0.3214(49)	-	-	-1.01(39)	-	0.41
ω_{m4}	2.2	0.3203(48)	-	-	-	-1.64(77)	0.42
$\omega_{2,0}$	2.2	0.3401(57)	-0.0185(52)	0.220(88)	-	-	0.73
$\omega_{3,0}$	2.1	0.3480(47)	-0.0201(36)	-0.264(89)	-1.03(28)	-	0.31

Table 4.7: Table of the best fits (selected by χ^2/dof and compatibility of the fitting values) for each weight including at least the strong coupling $\alpha_s(m_\tau^2)$ as a fitting variable. All fits have been performed using FOPT, except weights marked with a star ω^*, which have been fitted using the *Borel sum*.

4.1.7 Comparison

To create an overview of our previous results we have gathered the most compatible rows by hand. These are shown in table 4.7, which is composed of two parts:

- The upper three rows represent fits we found to have good properties for determining the strong coupling.
- The lower five rows are problematic fits due to too many OPE contributions, too low pinching or to terms proportional to x.

We have found that the kinematic weight is in excellent agreement with the cubic ω_{cube} and Pich's optimal weight $\omega_{3,0}$, fitted using the borel model. The fitted parameters from the kinematic weight (α_s, c_6 and c_8) are all within error ranges and thus compatible. One fact that has to be investigated is the negative appearing sign for the gluon-condensate from the borel-sum of $\omega_{3,0}$.

4.1.8 Toni Pich 2006

4. ALEPH determination

Toni built moments with five different weights:

$$\omega_{kl(x)} = (1-x)^{2+k}x^l(1+x) \quad \text{with} \quad (k,l) = (0,0),(1,0),(1,1),(1,2),(1,3) \tag{4.1.6}$$

He always fitted weight combinations, which we do not include.

5. Optimal moments

Used single moments

$$\omega^{(n,m)}(x) = (1-x)^n \sum_{k=0}^{n}(k+1)x^k \quad \text{with} \quad (n,m) = (1,0),(1,1),(1,2),(1,3),(1,4),(1,5),(2,0),(2,1 \tag{4.1.7}$$

but omitted NPT corrections! He fitted the kinematic weight with free α_s for $\omega(x)^{(2,1)}$. Later on he uses combined fits which is not in our interest. It is called optimal moments, because n stands for the pinching factor, which suppresses DV!

6. Including information from the s_0 dependence

Pich fits $A^{(2,0)}, A^{(2,1)}$ and $A^{(2,2)}$ separately for $s_{min} = 2\,GeV$. The corresponding weights with fitted OPE dimensions are given by:

$$\omega^{(2,0)} = (1-x)^2 \quad c_4, c_6 \tag{4.1.8}$$

$$\omega^{(2,1)} = \omega_\tau \quad c_6, c_8 \tag{4.1.9}$$

$$\omega^{(2,2)} = (1-x)^2(1+2x+x^2) = (x^2-1)^2 \quad c_8, c_{10} \tag{4.1.10}$$

Thus we can compare our results from the kinematic weight with his results and furthermore add $(1-x)^2$ to our fitting list?

Alpha is comparable, which just have a bigger error. For D6 and D8 we have to compare our definition of c_6, c_8 with his.

Chapter 5

Derivation of the used inverse covariance matrix from the Aleph data

While performing a **Generalized least squares** (GLS) we estimate our regression coefficients $\hat{\beta}$ as follows:

$$\hat{\beta} = \underset{b}{\operatorname{argmin}}(\mathbf{y} - \mathbf{X}\mathbf{b})^{T} \cdot^{-1} (\mathbf{y} - \mathbf{X}\mathbf{b}), \tag{5.0.1}$$

with **b** being an candidate estimate of β, **X** being the design matrix, **y** being the response values and $\cdot^{-1}$ being the **inverse covariance matrix**.

The Aleph data includes the **standard error** (SE), which are equal to the **standard deviation** as per definition. Furthermore Aleph provides the **correlation coefficients** of the errors. We will use these two quantities in combination with **Gaussian error propagation** to derive derive an approximation of the covariance matrix.

5.1 Propagation of experimental errors and correlation

Let $\{f_k(x_1, x_2, \cdots x_n)\}$ be a set of m functions, which a linear combinations of n variables $x_1, x_2, \cdots x_n$ with combination coefficients $A_{k1}, A_{k2}, \cdots A_{kn}$, where

$k \in \{1, 2, \cdots, m\}$. Let the covariance matrix of x_n be denoted by

$$\Sigma^x = \begin{pmatrix} \sigma_1^2 & \sigma_{12} & \sigma_{13} & \cdots \\ \sigma_{12} & \sigma_2^2 & \sigma_{23} & \cdots \\ \sigma_{13} & \sigma_{23} & \sigma_3^2 & \cdots \\ \vdots & \vdots & \vdots & \ddots \end{pmatrix}. \tag{5.1.1}$$

Then the covariance matrix of the functions Σ^f is given by

$$\Sigma^f_{ij} = \sum_k^n \sum_l^n A_{ik} \sum_{kl}^x A_{jl}, \quad \Sigma^f = A\Sigma^x A^T. \tag{5.1.2}$$

In our case we are dealing with non-linear functions, which we will linearized with the help of the **Taylor expansion**

$$f_k \approx f_k^0 + \sum_i^n \frac{\partial f_k}{\partial x_i} x_i, \quad f \approx f^0 + Jx. \tag{5.1.3}$$

Therefore, the propagation of error follows from the linear case, replacing the Jacobian matrix with the combination coefficients ($J = A$)

Chapter 6

Coefficients

6.1 β function

There are several conventions for defining the β coefficients, depending on a minus sign and/or a factor of two (if one substitues $\mu \to \mu^2$) in the β-function 2.1.12. We follow the convention from Pascual and Tarrach (except for the minus sign) and have taken the values from [7]

$$\beta_1 = \frac{1}{6}(11N_c - 2N_f), \tag{6.1.1}$$

$$\beta_2 = \frac{1}{12}(17N_c^2 - 5N_cN_f - 3C_fN_f), \tag{6.1.2}$$

$$\beta_3 = \frac{1}{32}\left(\frac{2857}{54}N_c^3 - \frac{1415}{54}N_c^2N_f + \frac{79}{54}N_cN_f^2 - \frac{205}{18}N_cC_fN_f + \frac{11}{9}C_fN_f^2 + C_f^2N_f\right), \tag{6.1.3}$$

$$\beta_4 = \frac{140599}{2304} + \frac{445}{16}\zeta_3, \tag{6.1.4}$$

where we used $N_f = 3$ and $N_c = 3$ for β_4.

6.2 Anomalous mass dimension

$$\gamma_1 = \frac{3}{2} C_f, \tag{6.2.1}$$

$$\gamma_2 = \frac{C_f}{48}(97N_c + 9C_f - 10N_f), \tag{6.2.2}$$

$$\gamma_3 = \frac{C_f}{32}\left[\frac{11413}{108}N_c^2 - \frac{129}{4}N_c C_f - \left(\frac{278}{27} + 24\zeta_3\right) N_c N_f + \frac{129}{2}C_f^2 - (23 - 24\zeta_3) C_f N_f - \frac{35}{27}N_f^2\right], \tag{6.2.3}$$

$$\gamma_4 = \frac{2977517}{20736} - \frac{9295}{216}\zeta_3 + \frac{135}{8}\zeta_4 - \frac{125}{6}\zeta_5, \tag{6.2.4}$$

where N_c is the number of colours, N_f the number of flavours and $C_f = (N_c^2 - 1)/2N_c$. We fixed furthermore fixed $N_f = 3$ and $N_c = 3$ for γ_4.

6.3 Adler function

Chapter 7

Källén-Lehmann spectral representation

In the second quantisation we applied latter operators $a_o^\dagger$ on the free vacuum $|0\rangle$ to obtain single particle states, carrying a momentum p

$$a_p^\dagger|0\rangle = \frac{1}{\sqrt{2E_p}}|\vec{p}\rangle, \tag{7.0.1}$$

where the factor $\sqrt{2E_p}$ is a convention resulting from the harmonic oscillator. The identity operator for one-particle state, which selects only single particle states is then given by

$$\mathbb{1} = \int \frac{d^3p}{(2\pi)^3}\frac{1}{2\omega_p}|\vec{p}\rangle\langle\vec{p}|. \tag{7.0.2}$$

The above complete set of one-particle states can be enhanced to include multiple-particle states, where we have to sum not only over all possible momentum states $|\vec{p}\rangle$, but over all possible multi-particle states and their enhanced states as well. If we define these state vectors as $\vec{X}$ we can express the complete set of one-and multiple-particle states as

$$\mathbb{1} = \sum_X \int d\prod_X |X\rangle\langle X|, \tag{7.0.3}$$

where we have to sum over all possible $|X\rangle$ single- or multi-particle states and integrate over the momentum $\vec{p}$ via

$$d\Pi_X \equiv \prod_{i\in X}\int \frac{d^3p_i}{(2\pi)^3}\frac{1}{2E_j}. \tag{7.0.4}$$

To get to the desired spectral decomposition we have to translate the Heisenberg operator $\phi(x)$ to its origin, like

$$\begin{aligned}\langle\Omega|\phi(x)|X\rangle &= \langle\Omega|e^{i\hat{P}x}e^{-i\hat{P}x}\phi(x)e^{i\hat{P}x}e^{-i\hat{P}x}|X\rangle \\ &= e^{-ip_X x}\langle\Omega|e^{-i\hat{P}x}\phi(x)e^{i\hat{P}x}|X\rangle \\ &= e^{-ip_X x}\langle\Omega|\phi(0)|X\rangle.\end{aligned} \tag{7.0.5}$$

Equally we can we can express $\phi(y)$ as

$$\langle X|\phi(y)|\Omega\rangle = e^{ipy}\langle\Omega|\phi(0)|\Omega\rangle. \tag{7.0.6}$$

With these expressions in hand we can spectral decompose the two-point function (**??**)

$$\begin{aligned}\langle\Omega|\phi(x)\phi(y)|0\rangle =& \sum_X \int d\Pi_X \langle\Omega|\phi(x)|X\rangle\langle X|\phi(y)|\Omega\rangle \\ =& \sum_X \int d\Pi_X e^{-ip_X(x-y)}\left|\langle\Omega|\phi(0)|X\rangle\right|^2 \\ =& \int \frac{d^4p}{(2\pi)^4}e^{-ip(x-y)}(2\pi)^3\left[\sum_X \int d\Pi_X 2\pi\delta^{(4)}(p-p_X)\left|\langle\Omega|\phi(0)|X\rangle\right|^2\right],\end{aligned} \tag{7.0.7}$$

where the term in the bracket is Lorentz invariant, implying that it depends only on the Lorentz-invariant measure p^2. The multi-particle states $|X\rangle$ have to have positive energy eigenstates $p^0 > 0$. Consequently we can define the *spectral function* as

$$\theta(p^0)\rho(p^2) \equiv \sum_X \int d\Pi_X 2\pi\delta^{(4)}(p-p_X)\left|\langle\Omega|\phi(0)|X\rangle\right|^2, \tag{7.0.8}$$

with $\rho(p^2)$ being the *spectral density*. The simple two-point function (**??**) can then be rewritten to

$$\begin{aligned}\langle\Omega|\phi(x)\phi(y)|\Omega\rangle &= \int \frac{d^4p}{(2\pi)^4}e^{-ip(x-y)}\theta(p^0)\rho(p^2) \\ &= \int_0^\infty dq^2\rho(q^2)D(x,y,q^2)\end{aligned} \tag{7.0.9}$$

with

$$\begin{aligned}D(x,y,m^2) &= \int \frac{d^3}{(2\pi)^3}\frac{1}{2E_p}e^{-ip(x-y)} \\ &= \int \frac{d^4p}{(2\pi)^3}e^{-ip(x-y)}\theta(p_0)\delta(p^2-m^2).\end{aligned} \tag{7.0.10}$$

$\rho(p^2)$ *spectral density*, $\rho(p^2) > 0$. The spectral function is a non-negative function, describing physically measurable particle states. Until now we have given the spectral function for our "simple" two-point function (**??**), but we can generalise the decomposition to the *Fourier transform* (FT) of the *time-ordered two-point function*

$$\Pi(p^2) = i\int \frac{d^4x}{(2\pi)^4} e^{-ixp}\langle\Omega|T\{\phi(x)\phi(0)\}|\Omega\rangle, \tag{7.0.11}$$

where we made use of the translation invariance of the correlator[1]. The time-ordered scalar correlator can then be expressed as

$$\begin{aligned}\Pi(p^2) &= i\int \frac{d^4x}{(2\pi)^4} e^{-ixp}\left[\theta(x^0-0)\langle\Omega|T\{\phi(x)\phi(0)\}|\Omega\rangle + \theta(y^0-0)\langle\Omega|T\{\phi(x)\phi(0)\}|\Omega\rangle\right]\\ &= i\int \frac{d^4x}{(2\pi)^4} e^{-ixp}\int_0^\infty dq^2\,\rho(q^2)\left[\theta(x^0-0)D(x,0,q^2) + \theta(y^0-0)D(0,x,q^2)\right]\\ &= i\int \frac{d^4x}{(2\pi)^4} e^{-ixp}\int_0^\infty dq^2\,\rho(q^2)\int \frac{d^4p}{(2\pi)^4}\frac{i}{p^2-q^2-i\epsilon}e^{ipx}\end{aligned} \tag{7.0.12}$$

by making use of the mathematical identity[2]

$$\theta(x^0-y^0)D(x,y,q^2) + \theta(y^0-x^0)D(y,x,q^2) = \int \frac{d^4p}{(2\pi)^4}\frac{i}{p^2-q^2-i\epsilon}e^{ip(x-y)}. \tag{7.0.13}$$

The last line of is given by two cancelling Fourier transforms. Thus we recognise the Källén-Lehmann spectral decomposition of the scalar time-ordered two-point function

$$\Pi(p^2) = \int_0^\infty dq^2 \frac{i\rho(q^2)}{p^2-q^2-i\epsilon}. \tag{7.0.14}$$

Also notice that when applying the following mathematical identity

$$\operatorname{Im}\frac{1}{p^2-q^2+i\epsilon} = -\pi\delta(p^2-q^2) \tag{7.0.15}$$

that the spectral function can be given by the imaginary part of the correlator

$$\rho(p^2) = -\frac{1}{\pi}\operatorname{Im}\Pi(p^2). \tag{7.0.16}$$

The spectral function usually has a pole at one-particle states and a branch cut above the multi-particle state threshold. The branch cut is of high importance

[1] $\langle\Omega|\phi(x)\phi(y)|\Omega\rangle = \langle\Omega|e^{i\hat{P}y}\underbrace{e^{-i\hat{P}y}\phi(x)e^{i\hat{P}y}}_{x-y}\underbrace{e^{-i\hat{P}y}\phi(y)e^{i\hat{P}y}}_{=\phi(0)}e^{-i\hat{P}y}|\Omega\rangle = \langle\Omega|\phi(x-y)\phi(0)|\Omega\rangle$

[2] The identity should be known to the reader from the derivation of the Feynman propagator.

to us as the experimental detected spectral function is only accessible at the possible real axis, where the branch cut exists. We will further study these singularities with the following example of a toy-Lagrangian of two interacting scalar fields.

Chapter 8

Analytic Structure of the Spectral Function ϕ^4-theory Example

To analyse the singularities contained in the spectral function $\rho(s)$ we have a look at the following Lagrangian

$$\mathcal{L} = -\frac{1}{2}\phi(\partial_\mu\partial^\mu + M^2)\phi - \frac{1}{2}\pi(\partial_\mu\partial^\mu + M^2)\pi + \frac{\lambda}{2}\phi\pi^2. \tag{8.0.1}$$

The Lagrangian contains two fields ϕ and π, which interact via the interaction term $\lambda/2\phi\pi^2$. We now want to calculate the self-interaction of the ϕ-field, as shown in fig. 8.1, to first order. To do so we need an expression for the free propagator of the ϕ field

$$G_\phi = \frac{1}{p^2 - M^2 + i\epsilon}. \tag{8.0.2}$$

Furthermore we need the result of the Feynman loop-diagram given in fig. 8.1

$$\operatorname{Im}\mathcal{M}^{\text{Loop}} = \frac{\lambda^2}{32\pi}\sqrt{1 - 4\frac{m^2}{M^2}}\theta(M - 2m) \tag{8.0.3}$$

Summing over all possible self-energy graphs we get a geometric series

$$iG(p^2) = \frac{i}{p^2 - m_R^2 + \Sigma(p^2) + i\epsilon}, \tag{8.0.4}$$

Figure 8.1: Self energy

where we can plugin the free propagator and the result of the loop diagram of our toy-Lagrangian to get a typical spectral function

$$\begin{aligned}\rho(q^2) &= -\frac{1}{\pi}\,\mathrm{Im}\,\Pi(q^2) \\ &= \frac{1}{\pi}\,\mathrm{Im}\left[p^2 - M^2 + i\epsilon + \frac{\lambda^2}{32\pi}\sqrt{1-4\frac{m^2}{M^2}}\,\theta(M-2m)\right]^{-1} \\ &= \delta(q^2-M^2) + \theta(q^2-4m^2)\frac{\lambda^2}{32\pi^2}\frac{1}{(q^2-M^2)^2}\sqrt{\frac{q^2-4m^2}{q^2}},\end{aligned} \tag{8.0.5}$$

where we have used eq. 7.0.15.

Bibliography

[1] Gerard 't Hooft. "Dimensional regularization and the renormalization group". In: *Nucl. Phys.* B61 (1973), pp. 455–468. DOI: 10.1016/0550-3213(73)90376-3.

[2] Gerard 't Hooft and M. J. G. Veltman. "Regularization and Renormalization of Gauge Fields". In: *Nucl. Phys.* B44 (1972), pp. 189–213. DOI: 10.1016/0550-3213(72)90279-9.

[3] S. Aoki et al. "FLAG Review 2019". In: (2019). arXiv: 1902.08191 [hep-lat].

[4] P. A. Baikov, K. G. Chetyrkin, and Johann H. Kuhn. "Order alpha**4(s) QCD Corrections to Z and tau Decays". In: *Phys. Rev. Lett.* 101 (2008), p. 012002. DOI: 10.1103/PhysRevLett.101.012002. arXiv: 0801.1821 [hep-ph].

[5] Martin Beneke, Diogo Boito, and Matthias Jamin. "Perturbative expansion of tau hadronic spectral function moments and α_s extractions". In: *JHEP* 01 (2013), p. 125. DOI: 10.1007/JHEP01(2013)125. arXiv: 1210.8038 [hep-ph].

[6] Martin Beneke and Matthias Jamin. "alpha(s) and the tau hadronic width: fixed-order, contour-improved and higher-order perturbation theory". In: *JHEP* 09 (2008), p. 044. DOI: 10.1088/1126-6708/2008/09/044. arXiv: 0806.3156 [hep-ph].

[7] Diogo Boito. "QCD phenomenology with τ and charm decays". PhD thesis. Universitat Autònoma de Barcelona, Sept. 2011.

[8] Diogo Boito et al. "A new determination of α_s from hadronic τ decays". In: *Phys. Rev.* D84 (2011), p. 113006. DOI: 10.1103/PhysRevD.84.113006. arXiv: 1110.1127 [hep-ph].

[9] Diogo Boito et al. "Strong coupling from $e^+e^- \to$ hadrons below charm". In: *Phys. Rev.* D98.7 (2018), p. 074030. DOI: 10.1103/PhysRevD.98.074030. arXiv: 1805.08176 [hep-ph].

[10] Diogo Boito et al. "Strong coupling from the revised ALEPH data for hadronic τ decays". In: *Phys. Rev.* D91.3 (2015), p. 034003. DOI: 10.1103/PhysRevD.91.034003. arXiv: 1410.3528 [hep-ph].

[11] C. G. Bollini and J. J. Giambiagi. "Dimensional Renormalization: The Number of Dimensions as a Regularizing Parameter". In: *Nuovo Cim.* B12 (1972), pp. 20–26. DOI: 10.1007/BF02895558.

[12] E. Braaten, Stephan Narison, and A. Pich. "QCD analysis of the tau hadronic width". In: *Nucl. Phys.* B373 (1992), pp. 581–612. DOI: 10.1016/0550-3213(92)90267-F.

[13] David J. Broadhurst. "Chiral Symmetry Breaking and Perturbative QCD". In: *Phys. Lett.* 101B (1981), pp. 423–426. DOI: 10.1016/0370-2693(81)90167-2.

[14] Irinel Caprini and Jan Fischer. "alpha(s) from tau decays: Contour-improved versus fixed-order summation in a new QCD perturbation expansion". In: *Eur. Phys. J.* C64 (2009), pp. 35–45. DOI: 10.1140/epjc/s10052-009-1142-8. arXiv: 0906.5211 [hep-ph].

[15] Oscar Cata, Maarten Golterman, and Santi Peris. "Unraveling duality violations in hadronic tau decays". In: *Phys. Rev.* D77 (2008), p. 093006. DOI: 10.1103/PhysRevD.77.093006. arXiv: 0803.0246 [hep-ph].

[16] William Celmaster and Richard J. Gonsalves. "An Analytic Calculation of Higher Order Quantum Chromodynamic Corrections in e+ e- Annihilation". In: *Phys. Rev. Lett.* 44 (1980), p. 560. DOI: 10.1103/PhysRevLett.44.560.

[17] K. G. Chetyrkin, A. L. Kataev, and F. V. Tkachov. "Higher Order Corrections to Sigma-t (e+ e- —> Hadrons) in Quantum Chromodynamics". In: *Phys. Lett.* 85B (1979), pp. 277–279. DOI: 10.1016/0370-2693(79)90596-3.

[18] K. G. Chetyrkin, Johann H. Kuhn, and M. Steinhauser. "RunDec: A Mathematica package for running and decoupling of the strong coupling and quark masses". In: *Comput. Phys. Commun.* 133 (2000), pp. 43–

65. DOI: 10.1016/S0010-4655(00)00155-7. arXiv: hep-ph/0004189 [hep-ph].

[19] Pietro Colangelo and Alexander Khodjamirian. "QCD sum rules, a modern perspective". In: (2000), pp. 1495–1576. DOI: 10.1142/9789812810458_0033. arXiv: hep-ph/0010175 [hep-ph].

[20] M. Davier et al. "The Determination of alpha(s) from Tau Decays Revisited". In: *Eur. Phys. J.* C56 (2008), pp. 305–322. DOI: 10.1140/epjc/s10052-008-0666-7. arXiv: 0803.0979 [hep-ph].

[21] Michel Davier, Andreas Hocker, and Zhiqing Zhang. "ALEPH Tau Spectral Functions and QCD". In: *Nucl. Phys. Proc. Suppl.* 169 (2007). [,22(2007)], pp. 22–35. DOI: 10.1016/j.nuclphysbps.2007.02.109. arXiv: hep-ph/0701170 [hep-ph].

[22] Michel Davier, Andreas Höcker, and Zhiqing Zhang. "The physics of hadronic tau decays". In: *Rev. Mod. Phys.* 78 (4 Oct. 2006), pp. 1043–1109. DOI: 10.1103/RevModPhys.78.1043. URL: https://link.aps.org/doi/10.1103/RevModPhys.78.1043.

[23] Michel Davier et al. "Update of the ALEPH non-strange spectral functions from hadronic τ decays". In: *Eur. Phys. J.* C74.3 (2014), p. 2803. DOI: 10.1140/epjc/s10052-014-2803-9. arXiv: 1312.1501 [hep-ex].

[24] Alexandre Deur, Stanley J. Brodsky, and Guy F. de Teramond. "The QCD Running Coupling". In: *Prog. Part. Nucl. Phys.* 90 (2016), pp. 1–74. DOI: 10.1016/j.ppnp.2016.04.003. arXiv: 1604.08082 [hep-ph].

[25] Michael Dine and J. R. Sapirstein. "Higher Order QCD Corrections in e+ e- Annihilation". In: *Phys. Rev. Lett.* 43 (1979), p. 668. DOI: 10.1103/PhysRevLett.43.668.

[26] C. A. Dominguez. "Introduction to QCD sum rules". In: *Mod. Phys. Lett.* A28 (2013), p. 1360002. DOI: 10.1142/S021773231360002X. arXiv: 1305.7047 [hep-ph].

[27] L. D. Faddeev and V. N. Popov. "Feynman Diagrams for the Yang-Mills Field". In: *Phys. Lett.* B25 (1967). [,325(1967)], pp. 29–30. DOI: 10.1016/0370-2693(67)90067-6.

[28] H. Fritzsch, Murray Gell-Mann, and H. Leutwyler. "Advantages of the Color Octet Gluon Picture". In: *Phys. Lett.* 47B (1973), pp. 365–368. DOI: 10.1016/0370-2693(73)90625-4.

[29] M. Gell-Mann. "Quarks". In: *Acta Phys. Austriaca Suppl.* 9 (1972). [,5(2015)], pp. 733–761. DOI: 10.1142/9789814618113_0002,10.1007/978-3-7091-4034-5_20.

[30] S. G. Gorishnii, A. L. Kataev, and S. A. Larin. "The $O(\alpha_s^3)$-corrections to $\sigma_{tot}(e^+e^- \to hadrons)$ and $\Gamma(\tau^- \to \nu_\tau + hadrons)$ in QCD". In: *Phys. Lett.* B259 (1991), pp. 144–150. DOI: 10.1016/0370-2693(91)90149-K.

[31] D. J. Gross and Frank Wilczek. "Asymptotically Free Gauge Theories - I". In: *Phys. Rev.* D8 (1973), pp. 3633–3652. DOI: 10.1103/PhysRevD.8.3633.

[32] Florian Herren and Matthias Steinhauser. "Version 3 of RunDec and CRunDec". In: *Comput. Phys. Commun.* 224 (2018), pp. 333–345. DOI: 10.1016/j.cpc.2017.11.014. arXiv: 1703.03751 [hep-ph].

[33] Matthias Jamin. "Contour-improved versus fixed-order perturbation theory in hadronic tau decays". In: *JHEP* 09 (2005), p. 058. DOI: 10.1088/1126-6708/2005/09/058. arXiv: hep-ph/0509001 [hep-ph].

[34] Matthias Jamin. *QCD and Renormalisation Group Methods*. Lecture presented at Herbstschule für Hochenergiephysik Maria Laach. Sept. 2006.

[35] Matthias Jamin and Manfred Munz. "Current correlators to all orders in the quark masses". In: *Z. Phys.* C60 (1993), pp. 569–578. DOI: 10.1007/BF01560056. arXiv: hep-ph/9208201 [hep-ph].

[36] Gunnar Kallen. "On the definition of the Renormalization Constants in Quantum Electrodynamics". In: *Helv. Phys. Acta* 25 (417). [,509(1952)]. DOI: 10.1007/978-3-319-00627-7_90.

[37] Alexander Keshavarzi, Daisuke Nomura, and Thomas Teubner. "Muon $g-2$ and $\alpha(M_Z^2)$: a new data-based analysis". In: *Phys. Rev.* D97.11 (2018), p. 114025. DOI: 10.1103/PhysRevD.97.114025. arXiv: 1802.02995 [hep-ph].

[38] L. V. Lanin, V. P. Spiridonov, and K. G. Chetyrkin. "Contribution of Four Quark Condensates to Sum Rules for ρ and A1 Mesons. (In Russian)". In: *Yad. Fiz.* 44 (1986), pp. 1372–1374.

[39] F. Le Diberder and A. Pich. "Testing QCD with tau decays". In: *Phys. Lett.* B289 (1992), pp. 165–175. DOI: 10.1016/0370-2693(92)91380-R.

[40] H. Lehmann. "On the Properties of propagation functions and renormalization contants of quantized fields". In: *Nuovo Cim.* 11 (1954), pp. 342–357. DOI: 10.1007/BF02783624.

[41] H. Lehmann, K. Symanzik, and W. Zimmermann. "On the formulation of quantized field theories". In: *Nuovo Cim.* 1 (1955), pp. 205–225. DOI: 10.1007/BF02731765.

[42] Stephan Narison. "QCD spectral sum rules". In: *World Sci. Lect. Notes Phys.* 26 (1989), pp. 1–527.

[43] R. Tarrach P. Pascual. *QCD: Renormalization for the Practitioner*. Springer-Verlag, 1984.

[44] W. Pauli and F. Villars. "On the Invariant Regularization in Relativistic Quantum Theory". In: *Rev. Mod. Phys.* 21 (3 July 1949), pp. 434–444. DOI: 10.1103/RevModPhys.21.434. URL: https://link.aps.org/doi/10.1103/RevModPhys.21.434.

[45] Michael E. Peskin and Daniel V. Schroeder. *An Introduction to quantum field theory*. Reading, USA: Addison-Wesley, 1995. URL: http://www.slac.stanford.edu/~mpeskin/QFT.html.

[46] Antonio Pich. "Precision Tau Physics". In: *Prog. Part. Nucl. Phys.* 75 (2014), pp. 41–85. DOI: 10.1016/j.ppnp.2013.11.002. arXiv: 1310.7922 [hep-ph].

[47] Antonio Pich and Joaquim Prades. "Strange quark mass determination from Cabibbo suppressed tau decays". In: *JHEP* 10 (1999), p. 004. DOI: 10.1088/1126-6708/1999/10/004. arXiv: hep-ph/9909244 [hep-ph].

[48] Antonio Pich and Antonio Rodríguez-Sánchez. "Determination of the QCD coupling from ALEPH τ decay data". In: *Phys. Rev. D* 94 (3 Aug. 2016), p. 034027. DOI: 10.1103/PhysRevD.94.034027. URL: https://link.aps.org/doi/10.1103/PhysRevD.94.034027.

[49] H. David Politzer. "Reliable Perturbative Results for Strong Interactions?" In: *Phys. Rev. Lett.* 30 (1973). [,274(1973)], pp. 1346–1349. DOI: 10.1103/PhysRevLett.30.1346.

[50] Eduardo de Rafael. "An Introduction to sum rules in QCD: Course". In: *Probing the standard model of particle interactions. Proceedings, Summer School in Theoretical Physics, NATO Advanced Study Institute, 68th session, Les Houches, France, July 28-September 5, 1997. Pt. 1, 2*. 1997, pp. 1171–1218. arXiv: hep-ph/9802448 [hep-ph].

[51] S. Schael et al. "Branching ratios and spectral functions of tau decays: Final ALEPH measurements and physics implications". In: *Phys. Rept.* 421 (2005), pp. 191–284. DOI: 10.1016/j.physrep.2005.06.007. arXiv: hep-ex/0506072 [hep-ex].

[52] Barbara Schmidt and Matthias Steinhauser. "CRunDec: a C++ package for running and decoupling of the strong coupling and quark masses". In: *Comput. Phys. Commun.* 183 (2012), pp. 1845–1848. DOI: 10.1016/j.cpc.2012.03.023. arXiv: 1201.6149 [hep-ph].

[53] Felix Schwab. "Strange Quark Mass Determination From Sum Rules For Hadronic τ-Decays". German. MA thesis. somewhere, 2002.

[54] Matthew D. Schwartz. *Quantum Field Theory and the Standard Model*. Cambridge University Press, 2014. ISBN: 1107034736, 9781107034730. URL: http://www.cambridge.org/us/academic/subjects/physics/theoretical-physics-and-mathematical-physics/quantum-field-theory-and-standard-model.

[55] Mikhail A. Shifman, A. I. Vainshtein, and Valentin I. Zakharov. "QCD and Resonance Physics: Applications". In: *Nucl. Phys.* B147 (1979), pp. 448–518. DOI: 10.1016/0550-3213(79)90023-3.

[56] Mikhail A. Shifman, A. I. Vainshtein, and Valentin I. Zakharov. "QCD and Resonance Physics. Theoretical Foundations". In: *Nucl. Phys.* B147 (1979), pp. 385–447. DOI: 10.1016/0550-3213(79)90022-1.

[57] David M. Straub. *rundec-python*. https://github.com/DavidMStraub/rundec-python. 2016.

[58] Levan R. Surguladze and Mark A. Samuel. "Total hadronic cross-section in e+ e- annihilation at the four loop level of perturbative QCD". In: *Phys. Rev. Lett.* 66 (1991). [Erratum: Phys. Rev. Lett.66,2416(1991)], pp. 560–563.

[59] M. Tanabashi et al. "Review of Particle Physics". In: *Phys. Rev.* D98.3 (2018), p. 030001. DOI: 10.1103/PhysRevD.98.030001.

[60] Yung-Su Tsai. "Decay Correlations of Heavy Leptons in $e^+ + e^- \to l^+ + l^-$". In: *Phys. Rev. D* 4 (9 Nov. 1971), pp. 2821–2837. DOI: 10.1103/PhysRevD.4.2821. URL: https://link.aps.org/doi/10.1103/PhysRevD.4.2821.

[61] Steven Weinberg. "New approach to the renormalization group". In: *Phys. Rev.* D8 (1973), pp. 3497–3509. DOI: 10.1103/PhysRevD.8.3497.

[62] Steven Weinberg. "Nonabelian Gauge Theories of the Strong Interactions". In: *Phys. Rev. Lett.* 31 (1973), pp. 494–497. DOI: 10.1103/PhysRevLett.31.494.

[63] Steven Weinberg. "Phenomenological Lagrangians". In: *Physica* A96.1-2 (1979), pp. 327–340. DOI: 10.1016/0378-4371(79)90223-1.

[64] Steven Weinberg. *The quantum theory of fields. Vol. 2: Modern applications*. Cambridge University Press, 2013. ISBN: 9781139632478, 9780521670548, 9780521550024.

[65] Kenneth G. Wilson. "Confinement of quarks". In: *Phys. Rev. D* 10 (8 Oct. 1974), pp. 2445–2459. DOI: 10.1103/PhysRevD.10.2445. URL: https://link.aps.org/doi/10.1103/PhysRevD.10.2445.

[66] Kenneth G. Wilson. "Nonlagrangian models of current algebra". In: *Phys. Rev.* 179 (1969), pp. 1499–1512. DOI: 10.1103/PhysRev.179.1499.

[67] Francisco J. Yndurain. *The Theory of Quark and Gluon Interactions*. Theoretical and Mathematical Physics. Berlin, Germany: Springer, 2006. ISBN: 9783540332091, 9783540332107. DOI: 10.1007/3-540-33210-3.

[68] Roman Zwicky. "A brief Introduction to Dispersion Relations and Analyticity". In: *Proceedings, Quantum Field Theory at the Limits: from Strong Fields to Heavy Quarks (HQ 2016): Dubna, Russia, July 18-30, 2016*. 2017, pp. 93–120. DOI: 10.3204/DESY-PROC-2016-04/Zwicky. arXiv: 1610.06090 [hep-ph].

List of Abbreviations

NPT Non-Perturbative Theory, page 7

NP Non-Perturbative, page 7

OPE Operator Product Expansion, page 18

PT Perturbative Theory, page 7

QCD Quantum Chromodynamics, page 4

QFT Quantum Field Theory, page 3

RGE Renormalisation Group Equation, page 9

SM Standard Model, page 3

CHPT Chiral Perturbation Theory, page 7

LQCD Lattice Quantum Chromodynamics, page 8

QCDSR Quantum Chromodynamics Sum Rules, page 8